Author Manuscript

Author Manuscript

Author Manuscript

Author Manuscript

HHS Public Access

Author manuscript

Cell Rep. Author manuscript; available in PMC 2023 October 23.

Published in final edited form as:

Cell Rep. 2023 June 27; 42(6): 112578. doi:10.1016/j.celrep.2023.112578.

Mutant *IDH* regulates glycogen metabolism from early cartilage development to malignant chondrosarcoma formation

Sinthu Pathmanapan[1,2], **Raymond Poon**[1], **Tomasa Barrientos De Renshaw**[3], **Puviindran Nadesan**[3], **Makoto Nakagawa**[3], **Gireesh A. Seesankar**[1], **Adrian Kwan Ho Loe**[1], **Hongyuan H. Zhang**[3], **Joan J. Guinovart**[4], **Jordi Duran**[4], **Christopher B. Newgard**[5,6], **Jay S. Wunder**[7], **Benjamin A. Alman**[3,8,*]

[1]Developmental and Stem Cell Biology, Hospital for Sick Children, Toronto, ON, Canada

[2]Institute of Medical Science, University of Toronto, Toronto, ON, Canada

[3]Department of Orthopaedic Surgery, Duke University, Durham, NC, USA

[4]Institute for Research in Biomedicine (IRB Barcelona) Barcelona, Barcelona, Spain

[5]Department of Pharmacology & Cancer Biology, Duke University, Durham, NC, USA

[6]Sarah W. Stedman Nutrition and Metabolism Center and Duke Molecular Physiology Institute, Duke University Medical Center, Durham, NC, USA

[7]Lunenfeld-Tanenbaum Research Institute and the University Musculoskeletal Oncology Unit, Mount Sinai Hospital, Toronto, ON, Canada

[8]Lead contact

SUMMARY

Chondrosarcomas are the most common malignancy of cartilage and are associated with somatic mutations in isocitrate dehydrogenase 1 (*IDH1*) and *IDH2* genes. Somatic *IDH* mutations are also found in its benign precursor lesion, enchondromas, suggesting that *IDH* mutations are early events in malignant transformation. Human mutant *IDH* chondrosarcomas and mutant *Idh* mice that develop enchondromas investigated in our studies display glycogen deposition exclusively in mutant cells from *IDH* mutant chondrosarcomas and *Idh1* mutant murine growth plates. Pharmacologic blockade of glycogen utilization induces changes in tumor cell behavior, downstream energetic pathways, and tumor burden *in vitro* and *in vivo*. Mutant IDH1 interacts with hypoxia-inducible factor 1α (HIF1α) to regulate expression of key enzymes in glycogen

This is an open access article under the CC BY-NC-ND license (http://creativecommons.org/licenses/by-nc-nd/4.0/).

*Correspondence: ben.alman@duke.edu.

AUTHOR CONTRIBUTIONS

S.P., B.A.A., C.B.N., and J.S.W. conceived the idea of the study and designed the study. S.P., T.B.D.R., P.N., M.N., G.A.S., A.K.H.L., and H.H.Z. acquired the data from the study. S.P., J.S.W., B.A.A., and C.B.N. analyzed and interpreted data from the study. S.P., B.A.A., C.B.N., and J.S.W. drafted and revised the work.

SUPPLEMENTAL INFORMATION

Supplemental information can be found online at https://doi.org/10.1016/j.celrep.2023.112578.

DECLARATION OF INTERESTS

The authors declare no competing interests.

Author Manuscript Author Manuscript Author Manuscript Author Manuscript

metabolism. Here, we show a critical role for glycogen in enchondromas and chondrosarcomas, which is likely mediated through an interaction with mutant IDH1 and HIF1α.

In brief

Pathmanapan et al. show a role for glycogen stores in tumor growth and benign lesion formation in mutant *IDH1* human chondrosarcomas and in a mutant *Idh1* murine model of enchondroma development. Regulation of glycogen metabolism was shown to be mediated through an interaction with mutant IDH1 and HIF1α.

Graphical Abstract

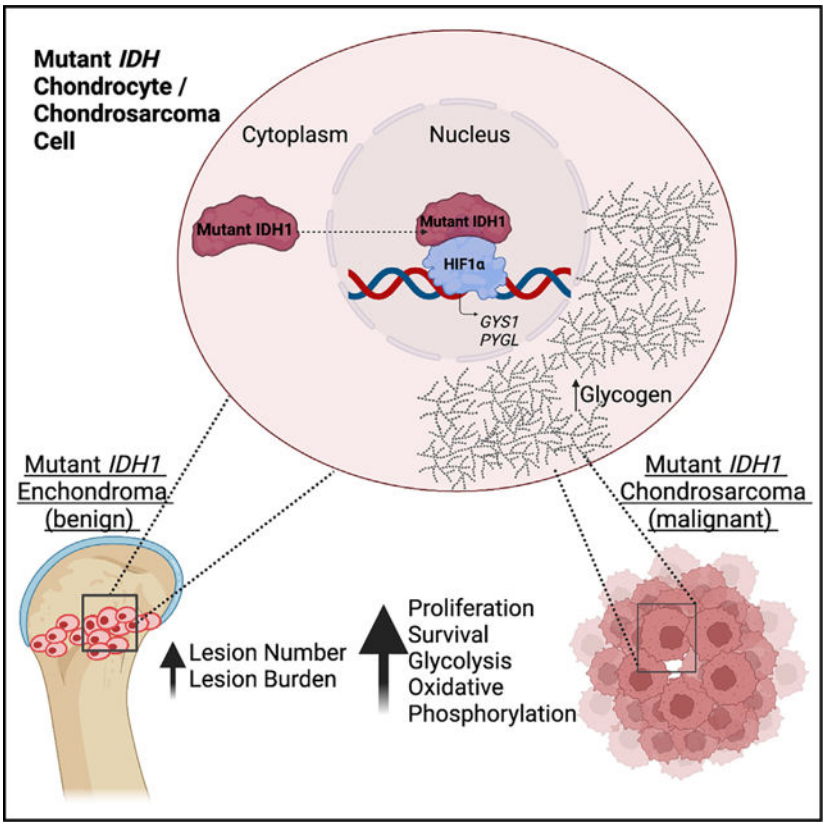

INTRODUCTION

Chondrosarcomas are the only cartilage malignancy of bone[1] and can develop from pre-existing benign cartilage lesions, enchondroma or osteochondroma, and progress to central or peripheral chondrosarcoma, respectively.[2] Deregulated chondrocyte differentiation in the growth plate driven by specific genetic mutations and deregulated developmental signaling pathways can lead to formation of its benign precursor lesion, enchondroma.[3–8] The majority of enchondromas harbor somatic isocitrate dehydrogenase (*IDH*) mutations,[9] and these mutations are present in half of chondrosarcomas,[9] suggesting that the abnormal *IDH* genes could potentially orchestrate early events in enchondroma and chondrosarcoma formation.

Author Manuscript Author Manuscript Author Manuscript Author Manuscript

Knocking in an *Idh1* mutation (*R132Q*) driven by cartilage-specific *Col2a1* regulatory elements causes a disrupted growth plate structure and defects in skeletal cartilage development, supporting the notion that *Idh1-KI R132Q* causes a delay in terminal differentiation.[10] Postnatal induction of mutant *Idh1-KI R132Q* was shown to be sufficient to initiate enchondroma-like lesion formation.[10] These findings are consistent with the notion that enchondromas are formed by a delay in growth plate terminal differentiation caused by a somatic mutaion.[6]

IDH mutations are found in several other neoplasms including gliomas, glioblastomas, and acute myeloid leukemia (AML).[11] *IDH1* and *−2* are enzymes located in the cytosol and mitochondria, respectively, and catalyze the interconversion of isocitrate and α-KG.[12] The mutant *IDH1* enzyme loses its ability to convert isocitrate to α-KG. Additionally, this enzyme gains a neomorphic function to produce D-2-hydroxyglutarate (D-2HG), which has been referred to as an oncometabolite due to its ability to inhibit α-KG-dependent dioxygenases including histone and DNA demethylases that regulate cellular epigenetics.[13]

Conventional chemotherapy and radiation are largely ineffective[14] in chondrosarcoma. While pharmacologic blockade of D-2HG production shows promising results in many tumor types,[15] data to date show variable effects on chondrosarcomas.[14,16,17] Some studies have shown that the mutant *IDH1* inhibitor ivosidenib was not able to influence tumorigenic cell behavior in chondrosarcoma cell cultures *in vitro*, as demonstrated by cell viability, colony formation, proliferation, and migration assays[14,17]; another showed that ivosidenib was able to suppress tumorigenic activity *in vitro*, as shown by colony formation, cell death, cell cycle, and migration assays.[16] Clinical data to date show safety, but studies are underpowered to assess a therapeutic response, and some patient on treatment showed progression.[18] These findings from pharmacological blockade of D-2HG in mutant *IDH* chondrosarcomas suggests that mechanisms other than D-2HG production in at least some of these tumors drives chondrosarcoma growth. A targeted metabolomics study highlighted several metabolic differences between mutant *IDH* and non-mutant chondrosarcomas, suggesting that glucose metabolism is enhanced in response to *IDH* mutations.[19] Since glycogen metabolism is responsible for the regulation of glucose storage, we aimed to examine mutant *IDH* regulation of glycogen metabolism in chondrosarcomas and early cartilage development.

Glycogen distribution is a metabolic feature of bone development in the growth plate, where chondrocytes proliferate.[20] Glycogen is abundant in the proliferative zone of the growth plate, and glycogen turnover is a feature of chondrocytes in the hypertrophic zone.[20] Large quantities of glycogen are found in various cancer cell lines such as breast, kidney, skin, and brain cell lines and in particular cells undergoing neoplastic transformation.[21] It is also known that glycogen promotes cancer cell survival in hypoxic environments through stabilization of hypoxia-inducible factor 1α (HIF1α).[22] HIF1α has been identified as a regulator of tumor glycogenesis by several studies.[22–26]

Here, we show that glycogen accumulates in mutant *IDH* chondrosarcomas. We demonstrate that a glycogen phosphorylase (PYGL) inhibitor drug, CP-91149, blocks glycogen degradation and impairs chondrosarcoma tumor growth. We also show that HIF1α is a

Author Manuscript Author Manuscript Author Manuscript Author Manuscript

transcriptional regulator of glycogen metabolism in mutant *IDH* chondrosarcomas and that mutant IDH and HIF1α interact to regulate gene expression. Moreover, glycogen synthase (*Gys1*) deletion in murine cartilage cells expressing a mutant *Idh* suppresses the neoplastic phenotype. Taken together, these data show that glycogen metabolism is a crucial metabolic pathway in enchondromas, chondrosarcomas, and the growth plate.

RESULTS

Glycogen deposition is present in mutant *IDH* chondrosarcoma patient tissues

Previous data showed that glucose metabolism and storage is enhanced in chondrosarcomas with an *IDH* mutation.[19] This raises the possibility that glucose storage, or, more specifically, glycogen metabolism, is activated in these tumors. We thus examined published microarray data from a cohort of chondrosarcomas[27,28] to determine if genes implicated in glycogen metabolism were expressed in these tumors. Several genes involved in glycogen metabolism and glycolysis were found to be elevated in chondrosarcomas harboring a mutant *IDH1* including *PYGL*, protein phosphatase 1 regulatory subunit 3C (*PPP1R3C*), and phosphoglucomutase 1 (*PGM1*), as well as a key glycolytic enzyme lactate dehydrogenase A (*LDHA*) (Figure S1). We next verified if glycogen was elevated in mutant *IDH* chondrosarcomas, using biochemical quantification, histology, and ultrastructural analysis. Examination of mutant *IDH* patient chondrosarcoma cells by electron microscopy showed accumulation of glycogen in the cytoplasm in mutant, but not non-mutant, tumor cells (Figures 1A and 1B). Glycogen appears as closely packed circular granules under electron microscopy,[29] which we observed in the mutant *IDH* chondrosarcoma patient cells (Figure 1B). To more readily distinguish glycogen granules from other organelles within cells in the figure, organelles were labeled as M for mitochondria, L for lysosome, and ER for rough endoplasmic reticulum, and an absence of glycogen granules can be seen in images (Figure 1A). Asterisks denote aggregates of glycogen pools in mutant *IDH* cells, and arrows in magnified insets indicate glycogen pools (Figure 1B). Measurement of glycogen levels in chondrosarcomas revealed significantly higher amounts in mutant *IDH1* and *IDH2* chondrosarcomas compared with non-mutant tumors (Figure 1C). Periodic acid-Schiff (PAS) and PAS with diastase (PAS-D) staining revealed glycogen deposits localized to the cytoplasm in mutant *IDH* chondrosarcoma tissues, which were absent in non-mutant chondrosarcoma tissues (Figures 1D and 1E).

Idh1-KI R132Q mutation leads to glycogen accumulation in the fetal growth plate

Next, we examined if a mutant *Idh1* in the murine growth plate leads to glycogen accumulation, similar to our observation in mutant *IDH* chondrosarcomas. A conditional *Idh1-KI* mouse line, which was previously generated,[10] was crossed with *Col2a1-Cre* transgenic mice to activate *Idh1-KI R132Q* ($Idh1^{LSL/wt}$) expression in chondrocytes. Hindlimb growth plates at developmental stage embryonic day 18.5 (E18.5) were used for analysis. PAS staining demonstrated glycogen accumulation in the resting, proliferative, and hypertrophic zones of E18.5 *Co-l2a1Cre;* $Idh1^{LSL/wt}$ ($Idh1^{LSL/wt}$*-KI*) proximal tibia growth plates (Figure 1F). The region of PAS staining was larger in the growth plates from $Idh1^{LSL/wt}$*-KI* mice compared with control growth plates (Figure 1G). PAS-D staining, which involves the addition of diastase enzyme, (Figure S2A), showed that the PAS

Author Manuscript Author Manuscript Author Manuscript Author Manuscript

staining was not a false positive due to other glycosylated proteins. We also measured expression of enzymes responsible for glycogen accumulation. Elevated levels of GYS1 (Figures 1H and 1I) were found in *Idh1*$^{LSL/wt}$*-KI* growth plates, whereas levels of the glycogenolytic enzyme PYGL remained unchanged (Figures 1J and 1K). Expression levels of genes regulating glycogen metabolism (*Gys1*, *Pygl*, *Pgm1*) (Figure 1L) were significantly upregulated in *Idh1*$^{LSL/wt}$*-KI* chondrocytes. This finding is consistent with the enhanced glycogen accumulation observed in *Idh1* mutant cells being due to activation of glycogen synthesis. The difference in PYGL protein levels in proximal tibia growth plate tissues and *Pygl* mRNA levels from sternum-derived chondrocytes *in vitro* (Figures 1J–1L) may be due to changes in glycogen flux metabolism that chondrocytes undergo once they are dissociated and plated *in vitro* (Figure 1L). Additionally, genes involved in glycolysis (*Glut1*, *Hk2*, *Ldha*) (Figure S2B) were also upregulated in *Idh1*$^{LSL/wt}$*-KI* chondrocytes.

Pharmacological blockade of glycogen utilization impairs glycolysis and oxidative phosphorylation in mutant *IDH* chondrosarcomas

To examine the impact of glycogen stores on tumorigenesis and tumor cell behavior, primary patient mutant *IDH* chondrosarcoma cell lines were studied *in vitro* using the PYGL allosteric inhibitor drug CP-91149. Previous studies showed that this drug affected proliferation and invasion in other cancer cell lines *in vitro*.[23,30] Growth of mutant *IDH* chondrosarcoma cells displayed dose-dependent sensitivity to the CP-91149 inhibitor drug (50–100 μM) using the MTT assay and 96 h of treatment (Figure 2A). 82.5 μM CP-91149 was optimized as the drug concentration to effectively block glycogenolysis (Figures 2B and S3). By testing various concentrations of CP-91149 on patient cell lines, we determined that 75–90 μM resulted in significant glycogen accumulation, thus suggesting that this range effectively inhibits glycogen utilization (Figure S3). Glycogenolysis blockade reduced BrdU incorporation and promoted apoptosis, as demonstrated by TUNEL staining (Figures 2C–2D), a finding that is consistent with glycogen reserves contributing to tumor cell viability, proliferation, and survival. There were no changes in cell viability, proliferation, or survival in non-mutant chondrosarcoma cell lines when treated with CP-91149 (Figures S4A– S4D), confirming that mutant *IDH* cells are more sensitive to glycogen blockade. This suggests that dysregulated glycogen metabolism is linked to the *IDH* mutation.

Glycogen reserve carbon and/or glucose carbon can be shunted into lactate via glycolysis,[31,32] a mode of energy production in many tumor cells.[32–34] Lactate levels were elevated in mutant *IDH* chondrosarcomas compared with non-mutant chondrosarcomas in data from a previously published metabolic study.[19] Relative intracellular and extracellular lactate levels were quantified using a luciferase bioluminescent assay. Three primary chondrosarcoma cell lines displayed a reduction in extracellular lactate levels upon treatment with CP-91149 (Figure 2E). Four cell lines displayed a reduction in intracellular lactate levels upon treatment with CP-91149 for 8 h (Figure 2F). This suggests that glycogenolysis fuels glycolysis for tumor cell energy production. Next, to assess how glycogenolysis blockade may affect metabolic function of chondrosarcoma cells in real time, we used the Seahorse XF Analyzer to measure two key metabolic pathways, glycolysis and oxidative metabolism. We found that pharmacological blockade of glycogen caused a significant reduction in the extracellular acidification rate (ECAR) in mutant *IDH*

Author Manuscript Author Manuscript Author Manuscript Author Manuscript

patient chondrosarcoma cells. Untreated cells displayed a high glycolytic capacity, whereas CP-91149-treated cells displayed a reduced glycolytic profile (Figure 2G). Thus, blocking glycogen utilization in mutant *IDH* chondrosarcoma cells causes a substantial loss of glycolytic capacity. CP-91149 treatment also showed a reduction in oxygen consumption rate (OCR) (Figure 2H). These data suggest that blocking glycogen utilization in mutant *IDH* chondrosarcoma cells diminishes mitochondrial respiration rates as well. Non-mutant *IDH* chondrosarcoma cells treated with the CP-91149 inhibitor did not display differences in extracellular or intracellular lactate production (Figures S4E and S4F), thus suggesting that mutant *IDH* cells are more dependent on their glycogen stores for metabolic output compared with non-mutant cells. This result strongly suggests that downstream energetic pathways are partly dependent on glycogen in mutant *IDH* cells.

Pharmacological blockade of glycogen utilization impairs chondrosarcoma tumor growth *in vivo*, reduces proliferation, and induces cellular senescence

To examine the effects of inhibiting glycogen utilization on mutant *IDH* chondrosarcoma growth, we treated mice harboring patient-derived xenografts with CP-91149 *in vivo*. Each primary patient line was injected into the flank region of 10 NSG mice; five mice were treated with a vehicle control, and five mice were treated with 50 mg/kg[35] CP-91149, starting after tumors became palpable. 50 mg/kg CP-91149 was selected as an effective drug concentration reported to not produce symptomatic hypoglycemia.[35] Blockade of glycogen utilization significantly impaired mutant *IDH* chondrosarcoma tumor growth *in vivo* (Figures 3A–3D). PAS staining confirmed that CP-91149 treatment resulted in significant glycogen accumulation (Figure S5A), thus suggesting that the 50 mg/kg dose effectively inhibits glycogen breakdown. There was a reduction in BrdU incorporation in CP-91149-treated tumors (Figure 3E). CP-91149 treatment did increase DEC1, p21, p16, and phosphorylated p53 immunostaining, markers of cellular senescence (Figures 3E, S5B, and S5C). Interestingly, *in vitro* results suggest that mutant *IDH* chondrosarcoma cells display sensitivity to CP-91149 treatment via induction of apoptosis (Figure 2D); however, *in vivo* results suggest that mutant *IDH* chondrosarcomas display sensitivity to CP-91149 treatment via induction of cellular senescence (Figure 3E). These differences can arise due to changes in the tumor microenvironment or cell interactions between *in vitro* and *in vivo* systems.[36] These results collectively suggest that mutant *IDH* chondrosarcomas use glycogen for cell proliferation and identify glycogen metabolism as a potential target for chondrosarcoma therapy.

Gys1 deletion is sufficient to partially rescue *Idh1-KI* phenotype in embryonic development

To determine the effect of glycogen metabolism in cartilage and skeletal development, the glycogen synthesizing enzyme *Gys1* was genetically deleted in chondrocytes by crossing $Gys1^{fl/fl}$ mice with $Idh1^{LSL/wt}$[10] and *Col2a1Cre* mice. Genetic deletion of *Gys1* abolishes glycogen synthesis in chondrocytes, completely inhibiting the glycogen metabolism pathway. Mice in which a mutant *Idh1* is conditionally knocked in driven by *Col2a1Cre* expression develop enchondroma-like lesions.[10] Prenatal skeletons were harvested from E18.5 and prepared for whole-mount alizarin red and Alcian blue skeletal staining. *Col2a1Cre;* $Gys1^{fl/fl}$ (*Gys1*-conditional knockout [CKO])-deleted skeletons did not display a visible change in phenotype or change in embryo length (Figures S6A and

Author Manuscript Author Manuscript Author Manuscript Author Manuscript

S6B) compared with wild-type littermate controls. *Idh1*$^{LSL/wt}$*-KI* skeletons displayed a short-limbed phenotype reported by Hirata et al.[10] (Figures S7A and S7B). Interestingly, *Col2a1Cre; Idh1*$^{LSL/wt}$; *Gys1*$^{fl/fl}$ (*Idh1*$^{LSL/wt}$; *Gys1*-CKO) skeletons appear less deformed and possess a less severe phenotype than *Idh1*$^{LSL/wt}$*-KI* skeletons (Figure 4A). *Idh1*$^{LSL/wt}$; *Gys1*-CKO embryos also trended larger than *Idh1*$^{LSL/wt}$*-KI* embryos (Figure S6B). Accordingly, *Idh1*$^{LSL/wt}$*-KI* humerus and femur displayed a rise in percent mineralization that was rescued by *Idh1*$^{LSL/wt}$; *Gys1*-CKO mice (Figure 4B). Interestingly, mineralized bone length and total bone length measurements (Figures S7A and S7B) did not display the same rescue by the *Idh1*$^{LSL/wt}$; *Gys1*-CKO mice, suggesting that genetic deletion of *Gys1* may not affect these specific bone measurements. This potentially suggests that *Gys1* deletion only rescues bone mineralization relative to total bone length, otherwise known as percent mineralization. These results show that *Gys1* deletion partially rescues the mutant *Idh1* phenotype seen in early cartilage and skeletal development.

Changes in chondrocyte cytology and growth plate zone delineations were observed in the *Idh1*$^{LSL/wt}$; *Gys1*-CKO growth plate. Ectopic expression of COLX was found in *Idh1*$^{LSL/wt}$*-KI* growth plates but not in *Idh1*$^{LSL/wt}$; *Gys1*-CKO growth plates (Figure 4C). There is also a reduction of COLX length in *Idh1*$^{LSL/wt}$; *Gys1*-CKO growth plates compared with *Idh1*$^{LSL/wt}$*-KI* growth plates (Figures 4C and 4D). Restricted COLX expression upon *Gys1* deletion suggests restoration of the normal chondrocyte differentiation process. In contrast, the disrupted columnar structure of chondrocytes in the proliferative zone (Figure 4E) was not rescued by *Gys1* deletion. PAS staining was used to confirm that *Gys1* deletion restricted glycogen storage in the growth plate (Figure 4F). Overall, these data suggest that *Gys1* deletion partially rescues the growth plate phenotype in mutant *Idh1* animals.

Gys1 deletion reduces the size and number of enchondroma-like cartilage lesions in mice expressing a mutant *Idh1*

To determine the role of glycogen metabolism in postnatal mutant *Idh1* enchondroma-like lesion formation, we generated *Col2a1Cre-ERT2; Idh1*$^{LSL/wt}$; *Gys1*$^{fl/fl}$ mice in which mutant *Idh1-KI R132Q* and *Gys1* deletions were simultaneously induced by tamoxifen administration in *Col2a1*-expressing cells. Tamoxifen was administered via intraperitoneal injection for 10 days at 100 mg/kg body weight/day at 4 weeks of age, and the enchondroma-like phenotypes of adult growth plates were analyzed from 5-month-old mice, a time point when enchondroma-like lesion formation is stable in *Idh1*$^{LSL/wt}$ mice.[10,37] Enchondroma-like lesions still formed even in the absence of *Gys1* (Figure 4G); however, the number of lesions and total lesion burden were reduced in *Gys1*-deleted femur growth plates (Figures 4H and 4I). Lesions of smaller volumes and width were found in *Col2a1Cre-ERT2; Idh1*$^{LSL/wt}$; *Gys1*$^{fl/fl}$ growth plates compared with *Col2a1Cre; Idh1*$^{LSL/wt}$ mice (Figures 4J and 4K). Thus, inhibiting glycogen reduces enchondroma-like lesion formation in *Idh1*$^{LSL/wt}$ mice, showing that glycogen metabolism plays a role in the number and size of cartilage lesions.

HIF1α transcriptionally regulates glycogen metabolism in mutant *IDH* chondrosarcomas

D-2HG produced by mutant *IDH* can drive metabolic changes through stabilization of HIF1α.[38] For this reason, mutant *IDH* inhibitor drugs have been used to treat *IDH* mutant

Author Manuscript Author Manuscript Author Manuscript Author Manuscript

malignancies, resulting in lower D-2HG levels.[14,39–41] Interestingly, chondrosarcomas of a higher pathological grade have increased levels of HIF1α.[42] Thus, we wanted to examine if this drug could alter glycogenesis in mutant *IDH* chondrosarcomas. We found that although the mutant IDH1 inhibitor did not change tumor weight (Figure S8A), D-2HG levels were significantly reduced (Figure S8B) and glycogen and HIF1α levels were only minimally affected (Figures S8C and S8D) in tumors treated daily for 4 weeks with the mutant IDH1 inhibitor drug. This suggests that the mutant IDH1 inhibitor was not effective in lowering glycogen levels regulated by HIF1α. Additionally, we examined if D-2HG levels can induce HIF1α expression through gene expression analysis of HIF1α target genes, *Glut1*, *Hk2*, and *Ldha* (Figure S9), in primary mouse chondrocytes treated with cell-permeable D-2HG (100 μM) for 4 days. HIF1α target gene expression remained unchanged even with D-2HG treatment, as well as expression of glycogen metabolism genes, *Gys1* and *Pgm1* (Figure S9). Thus, we concluded that D-2HG treatment does not lead to increased HIF1α expression levels in chondrocytes. This suggests that HIF1α may be functioning independently from D-2HG. Since glycogen can promote cancer cell survival in hypoxic environments through stabilization of HIF1α[22] and HIF1α can be a regulator of tumor glycogenesis,[22–26] we explored the possibility of HIF1α being a transcriptional regulator of glycogen metabolism in mutant *IDH* chondrosarcomas.

Analysis of published gene expression data shows elevated *HIF1α* levels in mutant *IDH1* chondrosarcomas (Figure 5A). Western blot analysis of the stable mutant *IDH1* chondrosarcoma cell line JJ012, treated with 0.5 mM dimethyloxallyl glycine (DMOG) and 0.25 μM digoxin to stabilize and deplete HIF1α, respectively, shows depletion of HIF1α, total PYGL, pPYGL, GYS1, and IDH1 protein levels when HIF1α is depleted (Figures 5B and S10). Thus, *IDH* mutant chondrosarcomas display higher HIF1α gene expression levels than non-mutant tumors, and HIF1α depletion results in the downregulation of key glycogen regulatory enzymes. To determine if HIF1α acts as a regulator of glycogen metabolism in primary patient chondrosarcoma cell lines, we treated mutant *IDH* chondrosarcoma cells with 0.5 μM digoxin and found reduced expression of HIF1α target genes, *PDK1* and *VEGF*, confirming that HIF1α was successfully depleted in these cell lines (Figure 5C). HIF1α depletion was also accompanied by reduced expression of glycogen metabolism genes, *GYS1*, *PYGL*, and *PPP1R3C*, in all four patient cell lines (Figure 5D). Interestingly, IDH1 protein and gene expression levels were downregulated upon HIF1α depletion by digoxin treatment (Figures 5B and 5D). To further support HIF1α regulation of IDH1, we found that upon treatment of HT1080 cells with DMOG to induce hypoxia, nuclear mutant IDH1 levels were elevated compared with DMSO-treated control cells (Figures S11A and S11B). Additionally, digoxin treatment for 24 h to suppress HIF1α protein showed a reduction in mutant IDH1 and HIF1α nuclear immunostaining intensity levels (Figures S11A and S11B). Chromatin immunoprecipitation (ChIP) of HIF1α and IDH1 shows that these proteins are enriched in the IDH1 hypoxia response element (HRE) promoter region in mutant $IDH1^{R132G}$ JJ012 chromatin (Figures S12 and S13F). These results suggest that HIF1α is a regulator of *IDH1* at the transcriptional level. This mechanism raises the possibility of a feedback mechanism between HIF1α and IDH in this cell type.

Author Manuscript Author Manuscript Author Manuscript Author Manuscript

HIF1α regulates glycogen metabolism in *Idh1-KI* chondrocytes and in the fetal growth plate

To determine if glycogen accumulation (Figures 1F and 1G) is mediated by HIF1α stabilization in *Idh1* mutant growth plates, we performed genetic and pharmacological ablation studies of *Hif1α*. HIF1α staining was increased and located in the nucleus in *Col2a1Cre; Idh1*$^{LSL/wt}$ growth plate chondrocytes (Figures 6A and 6B) compared with control. Staining for the HIF1α target GLUT1 was also increased in the *Col2a1Cre; Idh1*$^{LSL/wt}$ growth plate (Figures 6C and 6D). These data confirm that upon mutation of *Idh1*, growth plates display stabilized hypoxic activity.

Idh1$^{LSL/wt}$ mice were then crossed with *Hif1α*$^{fl/fl}$ mice. Sternal chondrocytes were isolated from postnatal stage 4. *Hif1α* knockout efficiency was confirmed by analysis of HIF1α target genes (*Glut1*, *Hk2*, *Ldha*) (Figure 6E). Glycogen metabolism genes (*Gys1*, *Pygl*, *Pgm1*) were downregulated with *Hif1α* depletion (Figure 6F). *Ex vivo* explant organ cultures of E16.5 *Col2a1-Cre-ERT; Idh1*$^{LSL/wt}$ metatarsals displayed reduced glycogen (PAS) and HIF1α levels upon pharmacological blockade of HIF1α using 0.5 μM digoxin treatment (Figure 6G). These data suggest that HIF1α is a transcriptional regulator of glycogen metabolism and its regulatory genes in mutant *Idh1* growth plates and chondrocytes.

HIF1α and mutant IDH1 interact and transcriptionally regulate glycogen metabolism in mutant *IDH1* tumor cells

Although other studies show that mutant *IDH1*-driven D-2HG production causes HIF1α stabilization, it has not been established whether a direct relationship exists between mutant IDH1 and HIF1α. Thus, we wanted to explore the possibility of mutant IDH1 and HIF1α proteins directly interacting. Immunostaining of mutant *Idh1*$^{LSL/wt}$ growth plates with two different antibodies (a monoclonal IDH1 antibody and a monoclonal recognizing mutant IDH1 R132) displayed strong cytoplasmic and strong nuclear staining, whereas control growth plates displayed no nuclear staining (Figures 7A and 7B). While it is known that HIF1α translocates to the nucleus in response to hypoxia,[43] wild-type IDH1 is reported to localize to the cytoplasm only. We next performed nuclear fractionation and co-immunoprecipitation (coIP) experiments on stable mutant *IDH1* tumor cell lines. After coIP of HIF1α in the nuclear fraction, we detected the associated IDH1 protein by immunoblotting (Figures 7C and S14) in mutant *IDH1 R132C* HT1080 cells. Accordingly, coIP of IDH1 revealed an association with HIF1α in the nuclear fraction (Figures 7C and S14). This association was minimally demonstrated in the cytoplasmic fraction but was abundantly displayed in the nuclear fraction (Figures 7C and S14). Similarly, coIPs performed on the mutant *IDH1 R132G* JJ012 cell line also showed an association of IDH1 with HIF1α in the nuclear protein fraction (Figures S15 and S16). As a control, we performed coIPs on a human chondrocyte C28 cell line containing wild-type IDH1 protein, which produced no coIP signals to suggest that the wild-type IDH1 and HIF1α do not interact with one another (Figures S17 and S18). It is important to note that trace levels of α-actin were detected in the nuclear protein fraction, suggesting incomplete fractionation in the following coIPs (Figures S15–S18). To further confirm the HIF1α and mutant IDH1 interaction, upon hypoxia induction, IDH1 and HIF1α proteins were found to co-localize to the nucleus, as shown by immunofluorescence staining of JJ012 cells (Figures 7D and 7E)

Author Manuscript Author Manuscript Author Manuscript Author Manuscript

and in HT1080 cells that harbor a mutant *IDH1* (Figures S19A and S19B). As a control, immunofluorescence of IDH1 in C28 cells, which express a wild-type *IDH1*, displayed reduced nuclear staining, although cytoplasmic IDH1 and HIF1α levels were unsurprisingly elevated in hypoxic conditions (Figures S20A and S20B). This is consistent with the notion that IDH1 is located in the nucleus only in cells expressing a mutant *IDH1* (Figures 7D, 7E, and S11) and that IDH1 is primarily located in the cytoplasm in cells expressing a wild-type *IDH1* (Figures S20A and S20B). We also examined protein localization in mouse growth plates. Mutant *Idh1* proliferative chondrocytes displayed nuclear staining of IDH1 and co-localization with HIF1α (Figures S21A and S21B). Control growth plates expressing wild-type *Idh1* displayed reduced nuclear staining of IDH1 (Figures S21A and S21B). Taken together, these results are consistent with IDH1 co-localizing with HIF1α in the nucleus in mutant *Idh1* chondrocytes and mutant *IDH1* chondrosarcoma cells.

To determine if the mutant IDH1 and HIF1α proteins are transcriptional regulators of genes involved in glucose and glycogen metabolism, we performed ChIP-re-ChIP on mutant $IDH1^{R132G}$ JJ012 cells. Individual ChIP-qRT-PCRs display enrichment of mutant IDH1 and HIF1α on the indicated gene promoter regions containing the HRE (Table S4), confirming that mutant IDH1 and HIF1α individually localize to the nucleus and occupy specific promoter regions of glycogen metabolism and HIF1α target genes of JJ012 chromatin (Figures 7F and S13A–S13F). We confirmed these results by demonstrating a PCR product band at the appropriate base-pair length of each gene promoter, suggesting that HIF1α and mutant IDH1 occupy these promoter regions (Figures S13A–S13F). ChIP-re-ChIP-qRT-PCRs of HIF1α and mutant IDH1 show that HIF1α and mutant IDH1 co-occupy the HRE of promoter regions of the glycogen metabolism genes *GYS1* and *PGM1* (Figure 7G), suggesting that HIF1α and mutant IDH1 interact to transcriptionally regulate genes involved in this metabolic pathway. Mutant IDH1, HIF1α enrichment was also found at the *GLUT1*, *VEGFA*, and *IDH1* promoter regions (Figure 7G). Visible differences in enrichment between HIF1α target genes and glycogen metabolism genes in the ChIP-re-ChIP experiment (Figure 7G) may be due to the presence of other transcription factors or co-factors being bound to HIF1α or mutant IDH1, differences in stability of proteins, or differences in performance of respective antibodies. Mutant IDH1, HIF1α enrichment was also found at the *GLUT1*, *VEGFA*, and *IDH1* promoter regions (Figure 7G). Visible differences in enrichment between HIF1α target genes and glycogen metabolism genes in the ChIP-re-ChIP experiment (Figure 7G) may be due to the presence of other transcription factors or co-factors being bound to HIF1α or mutant IDH1, differences in stability of proteins, or differences in performance of respective antibodies. Despite the differences between what was found in re-ChIP experiments, our data are consistent with the notion that HIF1α and mutant IDH1 interact and co-operate with one another to regulate genes in glycogen metabolism. We also identified HIF1α as a transcriptional regulator of mutant *IDH1*, suggesting that mutant IDH1 is not only a HIF1α interacting protein but also a transcriptional product of HIF1α. These observations provide insight into how the *IDH1* mutational state alters cellular metabolism and how mutant IDH1 and HIF1α regulate glycogen metabolism in cartilage lesion formation and chondrosarcoma tumorigenesis.

Author Manuscript Author Manuscript Author Manuscript Author Manuscript

DISCUSSION

Here, we report that mutant *IDH* regulates glycogen deposition in mutant *IDH* chondrosarcoma and growth plate chondrocyte cells. The role of glycogen metabolism in chondrosarcoma tumorigenesis was investigated by blockade of glycogen utilization, which induced changes in tumor cell behavior, downstream energetic pathways, and tumor burden *in vitro* and *in vivo*. Further studies in cartilage and skeletal tissues with mutant IDH1 demonstrated that cartilaginous *Gys1* deletion partially rescued the *Idh1-KI* phenotype. We also found that cartilaginous *Gys1* deletion reduced enchondroma-like cartilage lesion formation in mice. Finally, we provide evidence suggesting a mechanism in which HIF1α and mutant IDH1 interact to regulate expression of key metabolic enzymes.

Glycogen metabolism is a recognized feature of cancer cells.[21] Genetic factors such as activation of oncogenes and changes in the tumor microenvironment such as hypoxia and acidosis can regulate cancer cell glycogen metabolism.[22] Interestingly, it was found that hypoxia induces accumulation of glycogen stores in cells starved for glucose, while normoxic cells exhibited a high rate of cell death after glucose removal.[22] This suggests that glycogen serves as an energy reservoir, and glycogenolysis allows hypoxia preconditioned cells to confront and survive glucose deprivation. It is possible that mutant *IDH* chondrosarcomas accumulate glycogen for a similar purpose: to act as a reservoir of energy in times of glucose deprivation.

Interestingly, we found increased expression of genes encoding enzymes of glycogen synthesis as well as glycogen utilization in the IDH mutant cells. Despite this apparent co-activation of the synthetic and degradative pathways, we found a net increase in glycogen stores in these cells. This might be due to the balance of production and utilization being skewed toward more production than utilization, resulting in glycogen accumulation. An alternative explanation is that at the point in time in which we are examining the cells, glycogen has accumulated, and it would be utilized at future time points. Our findings are reminiscent of earlier cancer cell line studies in which genes implicated in glycogen production and utilization are both upregulated.[23]

Cartilage development and the process of chondrocyte differentiation are tightly regulated by multiple signaling pathways. Glycogen presence in the growth plate has been established for over a century, with electron microscopy and histological analysis indicating that glycogen is present in proliferating and hypertrophic zones.[44] Roles for glucose metabolism have been reported in cartilage development. One study demonstrated with radiolabeled glucose that proliferating chondrocytes consumed less glucose than hypertrophic chondrocytes.[45,46] Conversely, another study showed that proliferating chondrocytes consumed more glucose than hypertrophic chondrocytes over time.[45,47] These findings suggest that glucose uptake is tightly controlled during cartilage development and is dynamic in different cartilage zones. Although our studies identified HIF1α as a regulator of glycogen metabolism, others have identified IGF1, IGF2, and GSK3β as regulators of glycogen metabolism.[48] Thus, glycogen metabolism can be regulated through many mechanisms. We found that the *Gys1* deletion alone in growth plates resulted in an increased length of the proliferating zone and a

Author Manuscript Author Manuscript Author Manuscript Author Manuscript

decreased length of the hypertrophic zone, showing an important role for glycogen in growth plate function.

Our results suggest that mutant IDH1 gains the ability to translocate into the nucleus and interact with HIF1α. In support of our finding, previous studies have reported nuclear mutant IDH1 immunostaining using the monoclonal mutant IDH1 R132 antibody in brain tumors.[49–51] While it is mentioned in these studies that nuclear mutant IDH1 staining may be due to *in vivo* localization of the mutant protein to the nucleus or by antigen diffusion,[49–51] these data support the notion raised in this study that mutant IDH1 can localize to the nucleus to interact with HIF1α, with the complex possibly serving as a transcriptional regulator of genes involved in glycogen metabolism. Furthermore, evidence from this work suggests that mutant IDH1 interacts with HIF1α to co-occupy the HRE within the promoters of glycogen metabolic and HIF1α target genes to aid in transcriptional regulation. It remains unknown whether mutant IDH1 interacts with HIF1α as a co-activator in a complex with other proteins or if mutant IDH1 directly interacts with HIF1α to enhance HIF1α binding to chromatin, thus enhancing the HIF1α transcriptional machinery. These data raise the possibility of more direct transcriptional regulation by a mutant IDH, which is an area for future investigation.

In support of our findings, our analysis of previously published mRNA microarray data[27,28] revealed increased gene expression levels of glycogen regulatory genes in mutant *IDH* chondrosarcomas, which was also found to correlate with poor patient survival (Figures S1B and S1C). Taken together, these data are constant with the notion that glycogen metabolism regulatory genes are critical in mutant *IDH* chondrosarcoma metabolism and are predictive of patient survival (Figures S1B and S1C). Our data further suggest that targeting glycogen metabolism in these cells could be developed as a therapeutic approach for slowing the growth of chondrosarcomas.

Limitations of the study

Patient-derived xenograft (PDX) treatment using the mutant IDH1 inhibitor drug (Figures S8A–S8D) was a pilot study. As there were no observed changes in tumor burden from this pilot study, we did not expand on this work with additional replicates. We did detect differences in D-2HG levels, but there was a less than 33% change in HIF1α and glycogen levels; therefore, it is possible that there are smaller changes that our study lacked the sensitivity to detect. Further characterization of the mutant IDH1 and HIF1α interaction using biochemical, computational modeling, and/or mutational studies to identify binding sites of these proteins was not undertaken in this work. While our studies suggest that mutant IDH1 and HIF1α interact in the nucleus to transcriptionally regulate glycogen metabolism, production of the wild-type IDH1 protein from one allele in the tumor cells cannot completely exclude the less likely possibility that wild-type IDH1 translocates to the nucleus and binds HIF1α. Additionally, we utilized pharmacological agents in this work, and these may have off-target effects.

Author Manuscript Author Manuscript Author Manuscript Author Manuscript

STAR★METHODS

RESOURCE AVAILABILITY

Lead contact—Further information and requests for resources and reagents should be directed to and will be fulfilled by the lead contact, Benjamin A. Alman (ben.alman@duke.edu).

Materials availability—This study did not generate new unique reagents.

Data and code availability

- Microscopy data reported in this paper will be shared by the lead contact upon request. This paper analyzes existing, publicly available data. These accession numbers for the datasets are listed in the key resources table and methods detail section.
- This paper does not report original code.
- Any additional information required to reanalyze the data reported in this paper is available from the lead contact upon request.

EXPERIMENTAL MODEL AND STUDY PARTICIPANT DETAILS

Mouse models—Animal studies were used according to the approved protocol by Institutional Animal Care and Use committee of Duke University and UHN Animal Resource Center. Male and female animals were used for mouse models. *Gys1*$^{fl/fl}$ mice,[53] *Idh1-KI R132Q*,[10,54] *Col2a1Cre*,[55] *Col2a1Cre-ERT2*,[56] and *Col2a1Cre-ERT* (The Jackson Laboratory, Bar Harbor, ME), *Hif1α*$^{fl/fl}$ mice,[57] and NOD scid gamma (NSG) mice[58] were used for studies. "*fl/fl*" genotype indicates homozygous floxed allele, or genetic knockout of specified gene. *Idh1*^{R132Q}*(LSL/WT)* mice[10,54] were crossed with *Col2a1Cre*[55] to generate *Idh1*^{R132Q}*(LSL/WT); Col2a1Cre* and wildtype littermate controls and embryo growth plates harvested at E18.5. *Idh1 R132Q* mice bear an *R132Q* mutation rather than an *R132H* mutation as previously clarified.[10] *Gys1*$^{fl/fl}$ mice were provided by Dr. Joan J Guinovart and Dr. Jordi Duran from Institute for Research in Biomedicine (IRB Barcelona) Barcelona, Barcelona, Spain.[53] These mice were crossed with *Idh1*^{R132Q} mice and *Col2a1Cre* mice to generate *Idh1*^{R132Q}*(LSL/WT); Gys1*$^{fl/fl}$; *Col2a1Cre* and *Idh1*^{R132Q}*(LSL/WT); Gys1*$^{+/+}$; *Col2a1Cre* and wildtype littermate controls and embryo growth plates were harvested at E18.5. "*+/+*" genotype indicates a wildtype or unmodified allele. *Gys1*$^{fl/fl}$ and *Idh1*^{R132Q} mice were crossed with *Col2a1Cre-ERT2* (The Jackson Laboratory, Bar Harbor, ME) to generate *Gys1*$^{fl/fl}$; *Idh1*^{R132Q}*(LSL/WT); Col2a1Cre-ERT2* and *Idh1*^{R132Q}*(LSL/WT); Col2a1Cre-ERT2* and wildtype littermate controls and adult growth plates were harvested at 5 months of age. Adult growth plates and enchondroma-like phenotypes were analyzed on 5-month-old mice. Tamoxifen (Sigma-Aldrich, 579002) was administered via intraperitoneal injection for 10 days at 100 mg/kg body weight/day at 4 weeks of age. Hindlimbs were harvested for histological analysis. *Idh1*^{R132Q} mice were crossed with *Col2a1Cre-ERT* to generate *Idh1*^{R132Q}*(LSL/WT); Col2a1Cre-ERT* and wildtype littermate controls and metatarsals were harvested at E16.5. Tamoxifen (Sigma-Aldrich, 579002) was injected at 20 mg/kg and 10 mg/kg progesterone (Thermo Fisher

Author Manuscript Author Manuscript Author Manuscript Author Manuscript

Scientific, AC225650050) at E12.5. *Idh1*^{R132Q} mice were crossed with *HIF1α*$^{fl/fl}$ mice to generate *Idh1*^{R132Q}*(LSL/WT); HIF1α*$^{fl/fl}$ and *Idh1*^{R132Q}*(LSL/WT); HIF1α*$^{+/+}$ and wildtype littermate controls and sternums were collected at postnatal stage day 4 mice. 0.5 million mutant *IDH* chondrosarcoma patient cells containing PBS and Matrigel (Corning, 356234) were subcutaneously injected into the flank region of 30 interleukin-2 receptor gamma chain (gamma)-null NOD/SCID (NSG) mice (UHN Animal Resource Center). See method details section on Patient derived xenograft (PDX) drug treatment for further details.

Primary patient chondrosarcoma cell lines—Primary chondrosarcoma cell lines were processed at the time of surgical excision and were handled according to the ethical guidelines of the host institutions, and with institutional review board (IRB) approval. Primary chondrosarcoma cell lines were dissociated and cultured.[59] Primary tumor samples were manually minced, and all visible clumps were removed. Enzymatic digestion followed at 37°C for 45 min with constant rotation using 10 mg/mL of collagenase IV (Worthington Biochemical Corporation, LS004189), 2.4 units/mL Dispase (Thermo Fisher Scientific, 17105041), 0.05% trypsin (Wisent Bioproducts, 325240EL). Cells were centrifuged at 1400 rpm for 5 min and washed 3 times in PBS. Cells were strained through 70-μm filters to remove remaining clumps. Collected cells were grown in high glucose Dulbecco's modified Eagle's medium (DMEM; Wisent 319–005-EL) supplemented with 10% inactivated fetal bovine serum (FBS; Wisent 080–150) and 1X Antibiotic-Antimycotic (ABAM; Thermo Fisher 15240062). Cells were grown at 37°C with 5% CO_2 in a humidified sterile incubator. The following study (01–0138-U) has received continued approval from the Mount Sinai Hospital Research Ethics Board for the usage of human samples for research. Human samples were handled according to and animal work complied with the IRB guidelines.

HT1080, JJ012, and C28 cell lines—HT1080 cells[60] were purchased from ATCC (ATCC, CCL-121) and harbors endogenous heterozygous expression of *IDH1 R132C* mutation. JJ012 cells[61] (RRID: CVCL_D605) were a gift from Dr. Joel A Block of Rush University and harbors endogenous heterozygous expression of *IDH1 R132G* mutation. C28 cells[62] were purchased from Sigma-Aldrich (Sigma-Aldrich, SCC043) and harbors wildtype *IDH1* and *IDH2*. HT1080, JJ012, and C28 cells were grown in high glucose Dulbecco's modified Eagle's medium (DMEM; Wisent 319–005-EL) supplemented with 10% inactivated fetal bovine serum (FBS; Wisent 080–150) and 1X Antibiotic-Antimycotic (ABAM; Thermo Fisher 15240062). Cells were grown at 37°C with 5% CO_2 in a humidified sterile incubator.

METHOD DETAILS

Sanger sequencing of mutant *IDH1* and *IDH2*—Chondrosarcoma xenograft tumors were genotyped by extracting genomic DNA (gDNA) using the DNeasy Blood and Tissue Kit (Qiagen, 69504) according to manufacturer's protocol. PCR amplification of exon 4 of *IDH1* and *IDH2* was completed using the KOD Hot Start DNA Polymerase (Sigma-Aldrich, 71086–3). The indicated primer pairs (Table S1) were used for PCR amplification of exon 4 and identification of the *IDH1 R132*-and *IDH2 R172*-mutations. PCR products were purified using QIAquick PCR Purification Kit (Qiagen, 28104) and sanger sequencing of DNA was performed to analyze the samples for *IDH1* and *IDH2* mutations with specified

Author Manuscript Author Manuscript Author Manuscript Author Manuscript

sequencing primers (Table S1). Sequencing results were analyzed on 4Peaks software to confirm mutational status of each tumor.

Transmission electron microscopy—Primary chondrosarcoma cells were grown in DMEM supplemented with 10% FBS and 1XABAM until 90% confluency was reached. Cells were washed with phosphate buffered saline (PBS), trypsinized, and pelleted. Fixing solution (2% PFA, 2.5% glutaraldehyde, 0.1M sodium cacodylate buffer) was carefully dropped on top cell pellet and stored at 4°C until pellet was ready to be embedded in resin. Images were taken using FEI Tecnai 20 transmission electron microscope.

Glycogen quantification—Abcam Glycogen Assay Kit II (Abcam, ab169558) was used to quantify glycogen levels in pulverized PDX chondrosarcomas and patient chondrosarcoma cells. 10mg of chondrosarcoma tissue/1 million cells were homogenized in water and boiled to inactivate enzymes. Glycogen was degraded to free glucose by addition of glucoamylase, and glucose was measured colorimetrically at OD450nm with a microplate reader. Mouse liver and human muscle tissues were used as positive controls. Glycogen in chondrosarcoma tissue and cell samples were normalized to tissue weight and cellular protein concentration respectively.

D-2-Hydroxyglutrate (D-2HG) quantification—D-2HG was analyzed by liquid chromatography-tandem mass spectrometry (LC/MS/MS). Tumor tissue from patient derived xenografts were collected. After adding 2-HG-2H4 (internal standard), the sample was dried under nitrogen and derivatized by (+)-O,O′-diacetyl-L-tartaric anhydride (DATAN) for measurement.

Periodic acid-schiff stain (PAS) & periodic acid-schiff plus diastase stain (PASD)—Glycogen was detected in tumor sections and growth plate sections after a standardized periodic acid-Schiff (PAS) and diastase (PASD) staining techniques, which was performed by TCP Histology Services. CaseViewer program was used for capturing images and quantification of the PAS and PASD staining. PAS-stained area of tissues was quantified and subtracted by the PASD stained area using CaseViewer Histology plugin, stained area was then normalized to cell number.

Western blotting—For western blotting, JJ012 cells were treated with 0.5mM Dimethyloxallyl Glycine (DMOG) (Cayman Chemical, 71210), 0.25μM Digoxin (Cayman Chemical, 22266), or Dimethyl sulfoxide (DMSO) (Thermo Fisher, 85190) control for 48 h in culture. RIPA buffer (10mM Tris-HCl pH 8.0, 1mM EDTA, 0.5mM EGTA, 1% Triton X-100, 0.1% sodium deoxycholate, 0.1% SDS, 140mM NaCl) supplemented with cOmplete protease inhibitor (Roche, 11873580001) was used for lysis. Pierce BCA Protein Assay Kit (Thermo Fisher, 23227) was used to quantify protein concentrations. 30μg of protein was denatured by boiling at 100°C for 5 min with 5X loading buffer. Proteins were resolved on 10% polyacrylamide gel and transferred onto ImmunoBlot PVDF membrane (Bio-Rad, 1620177). Membranes were blocked in 5% BSA (Thermo Fisher Scientific, 11020021) in TBST (blocking buffer) at room temperature for 1 h. The indicated primary antibodies (Table S2) were diluted in blocking buffer and added to blots and rotated at 4°C overnight. Blots were washed in TBST three times for 5 min at room temperature. Indicated secondary

Author Manuscript Author Manuscript Author Manuscript Author Manuscript

horseradish peroxidase (HRP) linked antibodies (Table S2), to match the species the primary antibody was raised in, were diluted in blocking buffer and rotated at room temperature for 1.5 h. Blots were washed in TBST three times for 5 min at room temperature. Blots were developed using chemiluminescence imaging using Immobilon Forte Western HRP substrate (Millipore, WBLUF0100). Some blots were stripped and reprobed using Restore PLUS Western Blot Stripping Buffer (Thermo Fisher, 46430). Quantitative densitometry analysis of relative protein expression levels were measured using ImageJ. Protein density measurements are displayed as relative measurements by normalization to beta-actin protein density measurements.

Real-time quantitative PCR (RT-qPCR)—For Real-Time quantitative PCR, primary chondrosarcoma cells were treated with 0.5μM Digoxin (Cayman Chemical, 22266), or DMSO control for 5 days in culture and cells were lysed and RNA was extracted using Norgen Biotek Corp Single Cell RNA Isolation Kit (Norgen Biotek Corp, 51800). 1000ng of RNA was synthesized into cDNA using BioRad iScript (BioRad, 1708890) and diluted to a final concentration of 5 ng/μL of cDNA. The following forward and reverse primers indicated (Table S3) for each gene, mRNA transcript, was designed using NCBI's PrimerBLAST for *Homo saipan* (human) and *Mus musculus* (mouse). SsoAdvanced Universal SYBR Green Supermix (BioRad, 1725272) was used to drive amplification. 2μL of cDNA (10ng) and 5μL of SYBR Green Mix, 0.4μM of forward primer, 0.4μM of reverse primer to a final volume of 10μL per PCR reaction was used. Relative gene expression was compared to DMSO control treated group for individual patient cell lines which were normalized to 1 was calculated and normalized to beta-actin using the $2^{-\Delta\Delta Ct}$ method.

MTT cell viability assay—10,000 patient chondrosarcoma cells were seeded in a 96 well culture plate and treated with DMSO control or 82.5μM CP-91149 drug (Selleckchem, S2717) for 94 h. Trevigen TACs MTT Cell Proliferation Assay (R&D Systems, 4890–025-K) was used to assess cell viability. Plate was read at 570nm in a microplate reader.

Bromodeoxyuridine (BrdU) cell proliferation assay—10,0000 patient chondrosarcoma cells were seeded and treated for 18 h with DMSO control or 82.5μM CP-91149 drug. 10μM of BrdU labeling reagent (Thermo Fisher Scientific, 000103) was added to each well, maintaining the DMSO or CP-91149 treatment simultaneously. For the rest of the assay, the Cell Proliferation ELISA, BrdU Kit (Roche, 11647229001) was used. After a 6-h BrdU pulse period (6-h BrdU pulse determined by calculating 30% of doubling time for primary chondrosarcoma cells) media was removed, cells were fixed with ethanol, cells were incubated with primary BrdU antibody for 90 min at room temperature, and substrate solution was added to develop color. Plate was read after 5 min at 370nm in microplate reader.

Terminal deoxynucleotidyl transferase dUTP nick-end labeling (TUNEL) staining—*In Situ* Cell Death Detection Kit, TMR red (Roche, 12156792910) was used for TUNEL staining *in vitro*. Patient chondrosarcoma cells were seeded with glass coverslips and treated with DMSO control or 82.5μM CP-91149 for 4 days. Cells were fixed with 4% PFA (Thermo Fisher Scientific, 043368.9L) for 1 h at room temperature. TUNEL reaction

Author Manuscript Author Manuscript Author Manuscript Author Manuscript

mixture was added per coverslip and 1:1000 DAPI (Thermo Fisher Scientific, 62248) was added. DNase treated cells were used as a positive control and DMSO control cells without TUNEL reaction mix treatment was used a negative control. Plates were incubated in the dark at 37°C for 60 min. Samples were analyzed under a fluorescence microscope.

Lactate quantification assay—Lactate-Glo Assay (Promega, J5021) was used to quantify lactate levels. 10,0000 chondrosarcoma patient cells were seeded in a 96 well plate in technical triplicates and treated with DMSO control or 82.5μM CP-91149 for 8 h. To quantify intracellular lactate levels, cells were lysed with 0.6N HCl, neutralized using 1M Tris, and lactate detection reagent (contains luciferin detection solution, reductase, reductase substrate, lactate dehydrogenase, and NAD) was added to each well. Plate was incubated for 60 min at room temperature and luminescence was recorded. To quantify extracellular lactate levels, media from each well was saved, and diluted 1/20 with PBS. Lactate detection reagent was added to each well containing diluted media, plate was incubated for 60 min at room temperature, and luminescence was recorded.

Seahorse assay—20,000 chondrosarcoma patient cells were seeded in a 96 well Seahorse plate in technical quadruplicates and treated with DMSO control or 82.5μM CP-91149 for 20 h. Plate was placed into Agilent Seahorse XF96 analyzer and placed in extracellular acidification rate (ECAR) and oxidative consumption rate (OCR) read programs for 2.5 h.

Patient derived xenograft (PDX) drug treatment—All human chondrosarcoma samples were handled according to the ethical guidelines of the host institutions. With institutional review board (IRB) approval, human chondrosarcoma tumor samples were obtained fresh from surgery. 0.5 million mutant *IDH* chondrosarcoma patient cells were subcutaneously injected into the flank region of 30 interleukin-2 receptor gamma chain (gamma)-null NOD/ SCID (NSG) mice (UHN Animal Resource Center). 4 chondrosarcoma patient cell lines were tested, 10 mice were injected per patient cell line, for a total of 20 mice for DMSO control treated group and 20 mice for CP-91149 treated group. For the mutant IDH1 inhibitor (Selleckchem, S8206), 1 chondrosarcoma patient cell line was tested, 20 mice were injected with the patient tumor cells, for a total of 10 mice for DMSO control treated group and 10 mice for mutant IDH1 inhibitor treated group. Tumor cell injection containing Matrigel (Corning, 356234) was injected into the left side flank region of each mouse. 2–3 weeks after xenograft establishment (0.5mm), mice were treated with DMSO control or CP-91149 drug (50 mg/kg) or mutant IDH1 inhibitor (150 mg/kg), 5 days a week by intraperitoneal (IP) injection for 2 weeks for CP-91149 treatment and for 4 weeks for mutant IDH1 inhibitor treatment. Every 2–3 days, tumor length and width measurements were taken for tumor volume measurements. After tumors reached a maximal tumor endpoint of 2.5cm, mice were injected with 10μL/g (volume/mouse weight) of BrdU labeling reagent (Invitrogen, 000103) by IP injection. 2 h later, mice were sacrificed. Tumors were weighed to determine tumor weight; final tumor length and width were measured for final tumor volume measurements. The following formula was used to calculate final tumor volume = ½ (length × width^2).

Author Manuscript Author Manuscript Author Manuscript Author Manuscript

Immunohistochemical staining—Tissues were fixed in 10% formalin for 24 h and processed for paraffin embedding. 5um sections were hydrated with xylene and ethanol (100–70%) washes. Tissues were blocked of endogenous peroxidase activity with 3% hydrogen peroxide in methanol. Chondrosarcoma patient tissues were subjected to antigen retrieval in a pressure cooker in a microwave for full pressure for 4 min in 10mM sodium citrate buffer (pH = 6). E18.5 murine growth plate tissues were subjected to antigen retrieval in a microwave on full power for 10 min in 10mM sodium citrate buffer (pH = 6). Metatarsal explant tissues were subjected to antigen retrieval in a pressure cooker in a microwave for full pressure for 3 min in 10mM sodium citrate buffer (pH = 6). Tissues were blocked in 2% bovine serum albumin (BSA) (Thermo Fisher Scientific, 11020021) & 5% goat serum (Thermo Fisher Scientific, 31872) with Avidin (Vector Laboratories, SP2001) for 1 h. The indicated antibodies and dilutions were used for tissues (Table S2) at 4°C overnight. The next day, appropriate secondary antibodies (Table S2) were added to sections to match the species the primary antibody was raised in with Biotin (Vector Laboratories, SP2001) for 2 h at room temperature. ABC reagent (Vector Labs, PK-4000) was added, and DAB solution (Vector Labs, SK-4100) was added to develop stains. Sections were dehydrated through a series of ethanol and xylene washes and mounted with Permount (Thermo Fisher, SP15–500).

Gene expression profiling data analysis—Chondrosarcoma gene expression data was previously published by another group in their identification of genes that determine disease progression.[27] The miRNA microarray data and chondrosarcoma sample information[28] E-MTAB-7264 (https://www.ebi.ac.uk/biostudies/arrayexpress/studies/E-MTAB-7264) were downloaded from the European Bioinformatics Institute database[52] [PMID: 31604924]. Microarray data was normalized using the RMA algorithm with the “oligo” package [PMID: 20688976]. Gene expression data was further scaled for the generation of heatmaps. For survival analysis, samples were grouped into high/low expression based on median gene expression and plotted using the “survminer” package.

Isolation and culture of primary chondrocytes—Mouse chondrocytes were micro-dissected from the sternum at postnatal stage day 4 from *Idh1-KI R132Q (LSL/WT); Hif1a*$^{fl/fl}$ and *Idh1-KI R132Q (LSL/WT); Hif1a*$^{+/+}$ and wildtype littermate controls. “*+/+*” genotype indicates a wildtype or unmodified allele. Chondrocytes were dissociated using Pronase (Roche, 11459643001) 1 mg/mL and two washes of Collagenase D (Thermo Fisher Scientific, 11088882001) 1.5 mg/mL and 0.5 mg/mL overnight. Cells were plated and placed in culture overnight.

Adenovirus transfection—Dissociated primary chondrocytes were transfected with 1 × 10^{10} PFU/mL titer Ad-CMV-Cre or Ad-GFP (Vector Biolabs, 1700, 1060) at 500 MOI in serum free DMEM overnight with 1XABAM. The next day virus was removed and DMEM supplemented with 10% FBS and 1XABAM was added to the plate, allowing cells to grow for an additional 2 days.

Ex-vivo* explant culture of metatarsals—Idh1-KI R132Q* and *Col2a1Cre-ERT* mice were crossed and injected with 20 mg/kg tamoxifen (Sigma-Aldrich, 579002) and 10

Author Manuscript Author Manuscript Author Manuscript Author Manuscript

mg/kg progesterone (Thermo Fisher Scientific, AC225650050) at embryo day 12.5 (E12.5). Mice were sacrificed at E16.5. Both hindlimbs of embryos were placed on nitrocellulose membranes (Thermo Fisher Scientific, 88024) for adhesion and treated with 0.5μM Digoxin (Cayman Chemical, 22266) or DMSO control for 5 days. Digoxin and DMSO were dissolved in the following media: 500mL *a*MEM (Thermo Fisher Scientific, 12571063), 5mL of 10,000 U/mL penicillin streptomycin (P/S) (Thermo Fisher Scientific, 15140122), 25mg ascorbic acid (Thermo Fisher Scientific, AC105021000), 108mg *B*-glycerophosphate (Cayman Chemical, 14405), 1g BSA (Thermo Fisher Scientific, 11020021). After 5-day treatment, hindlimbs were fixed with 10% formalin and placed overnight at 4°C. Tissues were washed with 70% EtOH and processed for paraffin embedding and sectioning.

Alizarin red & Alcian blue whole mount skeletal staining—E18.5 embryos were fixed in 95% EtOH overnight at room temperature. Samples were placed in acetone overnight and room temperature. Cartilage was stained by submerging the embryo in Alcian blue solution (0.03% w/v, 80% EtOH, 20% glacial acidic). On day 4, embryos were destained by incubating in 95% EtOH overnight. On day 5, embryos were stained in Alizarin red solution (0.005% w/v, 1% KOH) to stain for calcified bone. On day 6, skeletons were washed in 1% KOH for 3 days. After 3 days, 1% KOH was replaced with 1:1 of (1% KOH: 100% glycerol) and incubated in solution at room temperature. Samples were transferred to 100% glycerol for long term storage.

Alcian blue staining of growth plates—E18.5 growth plate tissue sections were rehydrated through a series of ethanol washes (100%–70%) and placed in Alcian blue solution pH 0.77. Tissues were placed in running water, then placed in nuclear fast red counterstain (Vector Laboratories, H3403500). Tissues were dehydrated through a series of ethanol washes and mounted using Permount (Thermo Fisher, SP15–500).

Quantification of enchondroma like lesions—Enchondroma like lesions were detected by Safranin O staining. Growth plates were deparaffinized and hydrated, and stained in Weigert's Iron Hematoxylin (Abcam, ab245882) for 5 min, dipped in 0.02% Fast Green for 1 min, 1% Safranin O for 10 min, and dehydrated through a series of ethanol washes. We stained 1 slide (2 sections, 10um) in every 5 slides to identify enchondroma like lesions. We then examined every section of each bone under the microscope to determine the number of sections each enchondroma lesion spans. Each section is 5um thick and the width of each lesion was determined by the number of sections the lesion spanned.[37,63] For every Safranin O stained section, we manually outlined each lesion and measured lesion area using the image processing software ImageJ. We estimated the tumor volume of each animal by adding up the lesion areas of every Safranin O stained section.

Nuclear protein fractionation—JJ012, HT1080, and C28 cells were treated with 1mM of DMOG (Cayman Chemical, 71210) for 24 h in culture to stabilize HIF1α protein and prevent degradation. Plates were simultaneously placed in a hypoxic incubator for 24 h. NE-PER Nuclear and Cytoplasmic Extraction Kit (Thermo Fisher, 78833) was used to preform nuclear protein fractionation as per manufacturer's protocol. Pierce BCA Protein

Author Manuscript Author Manuscript Author Manuscript Author Manuscript

Assay Kit (Thermo Fisher, 23227) was used to quantify cytoplasmic and nuclear protein concentrations.

Co-immunoprecipitations (Co-IPs)—Beads for the Co-IPs were prepared: 20μL of Dynabeads Protein G (Thermo Fisher Scientific, 10003D) and 20μL of Pierce Protein A (Thermo Fisher Scientific, 88845) magnetic beads were combined per IP tube and washed with 0.5% BSA (Thermo Fisher Scientific, 11020021) in PBS using a magnetic rack. 0.5% BSA was added to IP tubes with beads and 5μg of indicated HIF1α and IDH1 antibodies (Table S2) and normal rabbit IgG (Table S2). Tubes with beads and antibodies were placed on a rotator at 4°C for a minimum of 4 h to allow for antibody bead conjugation. Antibody bound beads rotating at 4°C were washed 3x in 0.5% NP40 buffer (50mM Tris, 150mM NaCl, 0.5% NP40, pH = 7.4) supplemented with cOmplete protease inhibitor. Cytoplasmic and nuclear protein fraction volumes were evenly divided into each immunoprecipitation tube of HIF1α and IDH1 antibodies and IgG. 70μg of protein was saved from each fraction for input. Lysate-bead-antibody tubes were incubated overnight at 4°C. The next day, beads were washed 4 times with NP40 buffer. Beads were eluted by adding 2x loading buffer to beads, boiling at 100°C for 5 min, and supernatant was saved. Supernatant was saved in −20°C until ready to resolve proteins on 10% polyacrylamide gel (see western blotting methods).

Immunofluorescence—For cells *in vitro*, 100,000 cells from JJ012, HT1080, and C28 cell lines were seeded on glass coverslips in a 12 well plate and grown in culture for 24 h. Cells were treated with 0.4μM Digoxin (Cayman Chemical, 22266), 1mM DMOG (Cayman Chemical, 71210), or DMSO control for 24 h. Cells were fixed with 4% PFA (Thermo Fisher Scientific, 043368.9L) for 20 min at room temperature, permeabilized with 0.1% Triton X-100 for 30 min at room temperature, and blocked with blocking buffer: 2% BSA (Thermo Fisher Scientific, 11020021), 5% goat serum (Thermo Fisher Scientific, 31872) for 1 h at room temperature. For tissue sections, 5μm sections were hydrated with xylene and ethanol (100–70%) washes for 5 min each and washed in water for 5 min. Tissues were blocked of endogenous peroxidase activity with 3% hydrogen peroxide in methanol. E18.5 murine growth plate tissues were subjected to antigen retrieval in a microwave on full power for 10 min in 10mM sodium citrate buffer (pH = 6). Indicated HIF1*a* and IDH1 primary antibodies (Table S2) were diluted in blocking buffer were added to coverslips or tissue sections overnight at 4°C. Indicated fluorochrome conjugated secondary antibodies (Table S2) were diluted in blocking buffer with 1:1000 DAPI was added for 1 h at room temperature in the dark. Coverslips or tissues were mounted on glass slides using fluoroshield mounting medium (Abcam, ab104135). Images were captured using Nikon Eclipse E1000 microscope. JJ012, HT1080, and C28 cells were imaged together at 40x magnification and growth plate tissue sections were imaged separately at 20x magnification. Quantification of immunofluorescence staining was performed on ImageJ to measure cell intensity density of selected nuclear and cytoplasmic regions of cells. Set measurement commands input on ImageJ include area, integrated density, and mean gray value measurements. Background fluorescence was corrected for in final cell intensity density measurement readouts. Three cells were quantified per immunofluorescence staining.

Author Manuscript Author Manuscript Author Manuscript Author Manuscript

Chromatin immunoprecipitation (ChIP) Re-ChIP—JJ012 cells were treated with 1mM of DMOG for 24 h in culture to stabilize HIF1α. Plates were simultaneously placed in a hypoxic incubator for 24 h. Beads for the ChIP were prepared: 35μL of Dynabeads Protein G (Invitrogen, 10003D) and 35μL of Pierce Protein A (Thermo Fisher, 88845) magnetic beads were mixed together per ChIP tube and washed in 0.5% BSA (Thermo Fisher Scientific, 11020021) in PBS using a magnetic rack. 0.5% BSA was added to IP tubes with beads and indicated HIF1α, IDH, and H3K4 antibodies (Table S2), and normal rabbit IgG (Table S2) to beads. Tubes with beads and antibodies were placed on a rotator at 4°C for a minimum of 4 h to allow for antibody bead conjugation. To harvest cells, 1% formaldehyde (Millipore Sigma, 1040021000) was added per plate to cross link proteins to cells and was rotated at room temperature for 10 min. 0.125M of glycine solution was added per plate to stop cross linking and was rotated for 5 min at room temperature. Cells were washed, scraped, and collected. Cells were counted using a hemocytometer. Lysis buffer 1 (50mM HEPES-KOH pH 7.5, 140mM NaCl, 1mM EDTA pH 8.0, 10% glycerol, 0.5% NP40, 0.25% Triton X-100) with protease inhibitor was used for cytoplasm lysis. Lysis buffer 2 (10mM Tris-HCl pH 8.0, 200mM NaCl, 1mM EDTA, 0.5mM EGTA) was used to lyse the nucleus. Lysis buffer 3 (10mM Tris-HCl pH 8.0, 100mM NaCl, 1mM EDTA, 0.5mM EGTA, 0.1% Sodium-deoxycholate, 0.5% N-lauroylsarcosine, 0.1% SDS) was used to resuspend the chromatin. Diagenode Bioruptor Sonicator was used at 4°C and set to high setting, 25 cycles, 30 s on, and 30 s off to sonicate chromatin. Sample was run on a 2% agarose gel to determine chromatin shearing efficiency and fragment size. Fragments ran at 200–500bps. Rest of the lysate was taken and 1/10 of the volume of 10% Triton X-100 was added to remove background. Lysate was equally aliquoted into ChIP tubes (~50 million cells per ChIP tube) containing prepared beads and antibodies and rotated overnight at 4°C. 10% of chromatin added per ChIP tube was saved as 10% input. A second set of beads were prepared containing the second set of re-ChIP antibodies HIF1α, IDH1, and normal rabbit IgG (Table S2) and were left rotating overnight at 4°C. For re-ChIP samples, beads were washed 3x in RIPA, 1x in Buffer III (0.2M LiCl, 1% IGEPAL, 1% sodium-deoxycholate, 1mM EDTA, 10mM Tris-HCl pH 8.0), and 3x in Tris-EDTA pH 8.0. For re-ChIP, complexes were gently eluted from each sample in 50μL of 10mM DTT for 30 min at 37°C. DTT was deactivated by adding 200μL of dilution buffer (1% SDS, 10mM EDTA pH 8.0, 50mM Tris-HCl pH 8.0, 0.1% Triton X-100). The second set of antibody bound beads were washed, and re-ChIP lysate was added and rotated overnight at 4°C. For regular ChIP samples, beads were washed 5x in RIPA, 2x in ammonium hydrogen carbonate, and eluted in elution buffer (0.1M $NaHCO_3$, 1% SDS, 20 mg/mL Proteinase K (Thermo Fisher Scientific, AM2542)) and incubated at 65°C overnight. For re-ChIP samples the same washing and elution steps as described above were used. After ChIP and re-ChIP samples were subjected to Proteinase K (20 mg/mL) treatment at 65°C overnight, phenol chloroform extraction was performed to clean up and recover ChIP and ChIP re-ChIP DNA. DNA pellets were resuspended in 50μL of water and stored in −20°C for long term storage. Two biological replicates of ChIP re-ChIP was completed using the JJ012 cell line.

ChIP re-ChIP primer design and data analysis—Reverse and forward primer sequences were designed for glycogen metabolism and known HIF1α target genes (Table S4) using Ensembl genome browser 109 to locate and download gene promoter sequences.

Author Manuscript Author Manuscript Author Manuscript Author Manuscript

Oligonucleotides were designed by locating the promotor sequence of each gene, locating the hypoxia response element (HRE) within each gene's promoter region, and designing oligonucleotides encompassing the HRE. The HRE binding motif of 5'-(A/G)CGTG-3′ was used to locate potential HIF1α, mutant IDH1 binding sites. Promoter location, location of potential HIF1α, mutant IDH1 binding sites, and base pair locations of oligonucleotides are included in primer sequences are listed in Table S4. 1:5 diluted ChIP re-ChIP DNA was used for RT-qPCR reactions (see real-time quantitative PCR methods section). Two biological replicates of ChIP re-ChIP experiments were analyzed by RT-qPCR. Samples were run as technical triplicates with all biological replicates in one plate. 10% input samples, IgG, and H3K4 samples were run on the same plate. Percent input correction method was used to analyze ChIP re-chIP data acquired from real-time quantitative PCR.

QUANTIFICATION AND STATISTICAL ANALYSIS

Statistical analyses were performed using GraphPad (La Jolla, CA, USA) Prism 9 Software. Data were presented as means and error bars representing standard deviations. Two-tailed Student's t-test, and one-way or two-way ANOVA with post hoc comparisons using the Tukey's honest significant difference (HSD) test for multiple comparisons was used for statistical analysis and determination of statistical significance. $p < 0.05$, *, denoted with asterisks, was determined as a significant p value.

Supplementary Material

Refer to Web version on PubMed Central for supplementary material.

ACKNOWLEDGMENTS

We thank Dr. Qingxia Wei for generation of xenografts from patient chondrosarcoma tissues. We also thank Dr. Joan J Guinovart and Dr. Jordi Duran for *Gys1*$^{fl/fl}$ mice shipment. We thank our funding sources, NIH R01 AR066765 and CIHR MOP-37913, for funding this study.

INCLUSION AND DIVERSITY

We support inclusive, diverse, and equitable conduct of research.

REFERENCES

1. Rozeman LB, Cleton-Jansen AM, and Hogendoorn PCW (2006). Pathology of primary malignant bone and cartilage tumours. Int. Orthop. 30, 437–444. 10.1007/s00264-006-0212-x. [PubMed: 16944143]
2. Bovée JVMG, Hogendoorn PCW, Wunder JS, and Alman BA (2010). Cartilage tumours and bone development: molecular pathology and possible therapeutic targets. Nat. Rev. Cancer 10, 481–488. 10.1038/nrc2869. [PubMed: 20535132]
3. Mackie EJ, Ahmed YA, Tatarczuch L, Chen KS, and Mirams M (2008). Endochondral ossification: how cartilage is converted into bone in the developing skeleton. Int. J. Biochem. Cell Biol. 40, 46–62. 10.1016/j.biocel.2007.06.009. [PubMed: 17659995]
4. Zhang H, and Alman BA (2021). Enchondromatosis and growth plate development. Curr. Osteoporos. Rep. 19, 40–49. 10.1007/s11914-020-00639-7. [PubMed: 33306166]
5. Hiemcke-Jiwa LS, and Bové e J. (2022). Biology of cartilage tumor family. Bone Cancer, 649–662. 10.1016/b978-0-12-821666-8.00020-7.

Author Manuscript Author Manuscript Author Manuscript Author Manuscript

6. Hopyan S., Gokgoz N., Poon R., Gensure RC, Yu C., Cole WG, Bell RS, Jüppner H., Andrulis IL, Wunder JS, and Alman BA (2002). A mutant PTH/PTHrP type I receptor in enchondromatosis. Nat. Genet. 30, 306–310. 10.1038/ng844. [PubMed: 11850620]
7. Tiet TD, Hopyan S., Nadesan P., Gokgoz N., Poon R., Lin AC, Yan T., Andrulis IL, Alman BA, and Wunder JS (2006). Constitutive Hedgehog signaling in chondrosarcoma up-regulates tumor cell proliferation. Am. J. Pathol. 168, 321–330. 10.2353/ajpath.2006.050001. [PubMed: 16400033]
8. Gelderblom H., Hogendoorn PCW, Dijkstra SD, van Rijswijk CS, Krol AD, Taminiau AHM, and Bové e JVMG (2008). The clinical approach towards chondrosarcoma. Oncologist 13, 320–329. 10.1634/theoncologist.2007-0237. [PubMed: 18378543]
9. Peterse EFP, Niessen B., Addie RD, de Jong Y., Cleven AHG, Kruisselbrink AB, van den Akker BEWM, Molenaar RJ, Cleton-Jansen AM, and Bovée JVMG (2018). Targeting glutaminolysis in chondrosarcoma in context of the IDH1/2 mutation. Br. J. Cancer 118, 1074–1083. 10.1038/s41416-018-0050-9. [PubMed: 29576625]
10. Hirata M., Sasaki M., Cairns RA, Inoue S., Puviindran V., Li WY, Snow BE, Jones LD, Wei Q., Sato S., et al. (2015). Mutant *IDH* is sufficient to initiate enchondromatosis in mice. Proc. Natl. Acad. Sci. USA 112, 2829–2834. 10.1073/pnas.1424400112. [PubMed: 25730874]
11. Amary MF, Bacsi K., Maggiani F., Damato S., Halai D., Berisha F., Pollock R., O'Donnell P., Grigoriadis A., Diss T., et al. (2011). IDH1 and IDH2 mutations are frequent events in central chondrosarcoma and central and periosteal chondromas but not in other mesenchymal tumours. J. Pathol. 224, 334–343. 10.1002/path.2913. [PubMed: 21598255]
12. Turkalp Z., Karamchandani J., and Das S. (2014). IDH mutation in glioma: new insights and promises for the future. JAMA Neurol. 71, 1319–1325. 10.1001/jamaneurol.2014.1205. [PubMed: 25155243]
13. Turcan S., Makarov V., Taranda J., Wang Y., Fabius AWM, Wu W., Zheng Y., El-Amine N., Haddock S., Nanjangud G., et al. (2018). Mutant-IDH1-dependent chromatin state reprogramming, reversibility, and persistence. Nat. Genet. 50, 62–72. 10.1038/s41588-017-0001-z. [PubMed: 29180699]
14. Suijker J., Oosting J., Koornneef A., Struys EA, Salomons GS, Schaap FG, Waaijer CJF, Wijers-Koster PM, Briaire-de Bruijn IH, Haazen L., et al. (2015). Inhibition of mutant IDH1 decreases D-2-HG levels without affecting tumorigenic properties of chondrosarcoma cell lines. Oncotarget 6, 12505–12519. 10.18632/oncotar-get.3723. [PubMed: 25895133]
15. Horbinski C. (2013). What do we know about IDH1/2 mutations so far, and how do we use it? Acta Neuropathol. 125, 621–636. 10.1007/s00401-013-1106-9. [PubMed: 23512379]
16. Li L., Paz AC, Wilky BA, Johnson B., Galoian K., Rosenberg A., Hu G., Tinoco G., Bodamer O., and Trent JC (2015). Treatment with a small molecule mutant IDH1 inhibitor suppresses tumorigenic activity and decreases production of the oncometabolite 2-hydroxyglutarate in human chondrosarcoma cells. PLoS One 10, e0133813. 10.1371/journal.pone.0133813.
17. Cleven AHG, Suijker J., Agrogiannis G., Briaire-de Bruijn IH, Frizzell N., Hoekstra AS, Wijers-Koster PM, Cleton-Jansen AM, and Bovée JVMG (2017). IDH1 or −2 mutations do not predict outcome and do not cause loss of 5-hydroxymethylcytosine or altered histone modifications in central chondrosarcomas. Clin. Sarcoma Res. 7, 8. 10.1186/s13569-017-0074-6. [PubMed: 28484589]
18. Tap WD, Villalobos VM, Cote GM, Burris H., Janku F., Mir O., Beeram M., Wagner AJ, Jiang L., Wu B., et al. (2020). Phase I study of the mutant IDH1 inhibitor Ivosidenib: safety and clinical activity in patients with advanced chondrosarcoma. J. Clin. Oncol. 38, 1693–1701. 10.1200/JCO.19.02492. [PubMed: 32208957]
19. Pathmanapan S., Ilkayeva O., Martin JT, Loe AKH, Zhang H., Zhang GF, Newgard CB, Wunder JS, and Alman BA (2021). Mutant IDH and non-mutant chondrosarcomas display distinct cellular metabolomes. Cancer Metab. 9, 13. 10.1186/s40170-021-00247-8. [PubMed: 33762012]
20. Brighton C. (1978). Normal bone formation. In Normal Bone Formation, pp. 136–189.
21. Rousset M., Zweibaum A., and Fogh J. (1981). Presence of glycogen and growth–related variations in 58 cultured huma tumor cell lines of various tissue origins. Cancer Res. 41, 1165–1170. [PubMed: 7459858]

Author Manuscript Author Manuscript Author Manuscript Author Manuscript

22. Pelletier J., Bellot G., Gounon P., Lacas-Gervais S., Pouyssé gur J., and Mazure NM (2012). Glycogen synthesis is induced in hypoxia by the hypoxia-inducible factor and promotes cancer cell survival. Front. Oncol. 2, 18. 10.3389/fonc.2012.00018. [PubMed: 22649778]

23. Favaro E., Bensaad K., Chong MG, Tennant DA, Ferguson DJP, Snell C., Steers G., Turley H., Li JL, Gu€nther UL, et al. (2012). Glucose utilization via glycogen phosphorylase sustains proliferation and prevents premature senescence in cancer cells. Cell Metab. 16, 751–764. 10.1016/j.cmet.2012.10.017. [PubMed: 23177934]

24. Sun RC, Dukhande VV, Zhou Z., Young LEA, Emanuelle S., Brainson CF, and Gentry MS (2019). Nuclear glycogenolysis modulates histone acetylation in human non-small cell lung cancers. Cell Metab. 30, 903–916.e7. 10.1016/j.cmet.2019.08.014. [PubMed: 31523006]

25. Pescador N., Villar D., Cifuentes D., Garcia-Rocha M., Ortiz-Barahona A., Vazquez S., Ordoñ ez A., Cuevas Y., Saez-Morales D., Garcia-Bermejo ML, et al. (2010). Hypoxia promotes glycogen accumulation through hypoxia inducible factor (HIF)-mediated induction of glycogen synthase 1. PLoS One 5, e9644. 10.1371/journal.pone0009644.

26. Chiavarina B., Whitaker-Menezes D., Migneco G., Martinez-Outschoorn UE, Pavlides S., Howell A., Tanowitz HB, Casimiro MC, Wang C., Pestell RG, et al. (2010). HIF1-alpha functions as a tumor promoter in cancer associated fibroblasts, and as a tumor suppressor in breast cancer cells: autophagy drives compartment-specific oncogenesis. Cell Cycle 9, 3534–3551. 10.4161/cc.9.17.12908. [PubMed: 20864819]

27. Nicolle R., Ayadi M., Gomez-Brouchet A., Armenoult L., Banneau G., Elarouci N., Tallegas M., Decouvelaere AV, Aubert S., Ré dini, F., et al. (2019). Integrated molecular characterization of chondrosarcoma reveals critical determinants of disease progression. Nat. Commun. 10, 4622. 10.1038/s41467-019-12525-7. [PubMed: 31604924]

28. Nabila E. (2018). E-MTAB-7265 - High-Throughput Sequencing of miRNA of Cartilage Tumors. https://www.ebi.ac.uk/arrayexpress/experiments/E-MTAB-7265/.

29. Revel P., and Whitney H. (1960). Identification of Glycogen of Thin Tissue in Electron Sections.

30. Curtis M., Kenny HA, Ashcroft B., Mukherjee A., Johnson A., Zhang Y., Helou Y., Batlle R., Liu X., Gutierrez N., et al. (2019). Fibroblasts mobilize tumor cell glycogen to promote proliferation and metastasis. Cell Metab. 29, 141–155.e9. 10.1016/j.cmet.2018.08.007. [PubMed: 30174305]

31. Shulman RG, and Rothman DL (2017). The glycogen shunt maintains glycolytic homeostasis and the Warburg effect in cancer. Trends Cancer 3, 761–767. 10.1016/j.trecan.2017.09.007. [PubMed: 29120752]

32. Jiang B. (2017). Aerobic glycolysis and high level of lactate in cancer metabolism and microenvironment. Genes Dis. 4, 25–27. 10.1016/j.gendis.2017.02.003. [PubMed: 30258905]

33. Warburg O. (1930). The Metabolism of Tumours: Investigations from the Kaiser Wilhelm Institute for Biology (Berlin-Dahlem (London, UK: Arnold Constable).

34. Otto Warburg B., Wind F., and Negelein N. (1923). The metabolism of tumors in the body. J. Gen. Physiol. 309, 397–519. 10.1097/00000441-193107000-00022.

35. Martin WH, Hoover DJ, Armento SJ, Stock IA, McPherson RK, Danley DE, Stevenson RW, Barrett EJ, and Treadway JL (1998). Discovery of a human liver glycogen phosphorylase inhibitor that lowers Blood glucose in vivo. Proc. Natl. Acad. Sci. USA 95, 1776–1781. [PubMed: 9465093]

36. Katt ME, Placone AL, Wong AD, Xu ZS, and Searson PC (2016). In vitro tumor models: advantages, disadvantages, variables, and selecting the right platform. Front. Bioeng. Biotechnol. 4, 12. 10.3389/fbioe.2016.00012. [PubMed: 26904541]

37. Zhang H., Puviindran V., Nadesan P., Ding X., Shen L., Tang YJ, Tsushima H., Yahara Y., Ban GI, Zhang GF, et al. (2022). Distinct roles of glutamine metabolism in benign and malignant cartilage tumors with IDH mutations. J. Bone Miner. Res. 37, 983–996. 10.1002/jbmr.4532. [PubMed: 35220602]

38. Dang L., Yen K., and Attar EC (2016). IDH mutations in cancer and progress toward development of targeted therapeutics. Ann. Oncol. 27, 599–608. 10.1093/annonc/mdw013. [PubMed: 27005468]

39. Li L., Paz AC, Wilky BA, Johnson B., Galoian K., Rosenberg A., Hu G., Tinoco G., Bodamer O., and Trent JC (2015). Treatment with a small molecule mutant IDH1 inhibitor suppresses

Author Manuscript Author Manuscript Author Manuscript Author Manuscript

tumorigenic activity and decreases production of the oncometabolite 2-hydroxyglutarate in human chondrosarcoma cells. PLoS One 10, e0133813. 10.1371/journal.pone.0133813.

40. Nakagawa M., Nakatani F., Matsunaga H., Seki T., Endo M., Ogawara Y., Machida Y., Katsumoto T., Yamagata K., Hattori A., et al. (2019). Selective inhibition of mutant IDH1 by DS-1001b ameliorates aberrant histone modifications and impairs tumor activity in chondrosarcoma. Oncogene 38, 6835–6849. 10.1038/s41388-019-0929-9. [PubMed: 31406254]
41. Popovici-Muller J., Lemieux R., Artin E., Saunders JO, Salituro FG, Travins J., Cianchetta G., Cai Z., Zhou D., Cui D., et al. (2018). Discovery of AG-120 (Ivosidenib): a first-in-class mutant IDH1 inhibitor for the treatment of IDH1 mutant cancers. ACS Med. Chem. Lett. 9, 300–305. 10.1021/acsmedchemlett.7b00421. [PubMed: 29670690]
42. Chen C., Zhou H., Wei F., Jiang L., Liu X., Liu Z., and Ma Q. (2011). Increased levels of hypoxia-inducible factor-1a are associated with Bcl-xL expression, tumor apoptosis, and clinical outcome in chondrosarcoma. J. Orthop. Res. 29, 143–151. 10.1002/jor.21193. [PubMed: 20661931]
43. Masoud GN, and Li W. (2015). HIF-1α pathway: role, regulation and intervention for cancer therapy. Acta Pharm. Sin. B 5, 378–389. 10.1016/j.apsb.2015.05.007. [PubMed: 26579469]
44. Godman GC, and Porter KR (1960). Chondrogenesis, studied with the electron microscope. J. Biophys. Biochem. Cytol. 8, 719–760. [PubMed: 13706207]
45. Hollander JM, and Zeng L. (2019). The emerging role of glucose metabolism in cartilage development. Curr. Osteoporos. Rep. 17, 59–69. 10.1007/s11914-019-00506-0. [PubMed: 30830516]
46. Ohara H., Tamayama T., Maemura K., Kanbara K., Hayasaki H., Abe M., and Watanabe M. (2001). Immunocytochemical demonstration of glucose transporters in epiphyseal growth plate chondrocytes of young rats in correlation with autoradiographic distribution of 2-deoxyglucose in chondrocytes of mice. Acta Histochem. 103, 365–378. 10.1078/0065-1281-00604. [PubMed: 11700943]
47. Rajpurohit R., Mansfield K., Ohyama K., Ewert D., and Shapiro IM (1999). Chondrocyte death is linked to development of a mitochondrial membrane permeability transition in the growth plate. J. Cell. Physiol. 179, 287–296. https://onlinelibrary.wiley.com/doi/10.1002/(SICI)1097-4652. [PubMed: 10228947]
48. Gillespie JR, Ulici V., Dupuis H., Higgs A., Dimattia A., Patel S., Woodgett JR, and Beier F. (2011). Deletion of glycogen synthase kinase-3 in cartilage results in up-regulation of glycogen synthase kinase-3 protein expression. Endocrinology 152, 1755–1766. 10.1210/en.2010-1412. [PubMed: 21325041]
49. Agarwal S., Sharma MC, Jha P., Pathak P., Suri V., Sarkar C., Chosdol K., Suri A., Kale SS, Mahapatra AK, and Jha P. (2013). Comparative study of IDH1 mutations in gliomas by immunohistochemistry and DNA sequencing. Neuro Oncol. 15, 718–726. 10.1093/neuonc/not015. [PubMed: 23486690]
50. Capper D., Weiβert S., Balss J., Habel A., Meyer J., Jä ger D., Ackermann U., Tessmer C., Korshunov A., Zentgraf H., et al. (2009). Characterization of R132H mutation-specific IDH1 antibody binding in brain tumors. Brain Pathol. 20, 245–254. 10.1111/j.1750-3639.2009.00352.x. [PubMed: 19903171]
51. Preusser M., Wöhrer A., Stary S., Hö ftberger R., Streubel B., and Hainfellner JA (2011). Value and limitations of immunohistochemistry and gene sequencing for detection of the IDH1-R132H mutation in diffuse glioma biopsy specimens. J. Neuropathol. Exp. Neurol. 70, 715–723. [PubMed: 21760534]
52. European Bioinformatics Institute database (EMBL-EBI).
53. Duran J., Saez I., Gruart A., Guinovart JJ, and Delgado-García JM (2013). Impairment in long-term memory formation and learning-dependent synaptic plasticity in mice lacking glycogen synthase in the brain. J. Cereb. Blood Flow Metab. 33, 550–556. 10.1038/jcbfm.2012.200. [PubMed: 23281428]
54. Sasaki M., Knobbe CB, Munger JC, Lind EF, Brenner D., Brüstle A., Harris IS, Holmes R., Wakeham A., Haight J., et al. (2012). IDH1(R132H) mutation increases murine haematopoietic progenitors and alters epigenetics. Nature 488, 656–659. 10.1038/nature11323. [PubMed: 22763442]

Author Manuscript Author Manuscript Author Manuscript Author Manuscript

55. Long F., Zhang XM, Karp S., Yang Y., and McMahon AP (2001). Genetic manipulation of hedgehog signaling in the endochondral skeleton reveals a direct role in the regulation of chondrocyte proliferation. Development 128, 5099–5108. [PubMed: 11748145]
56. Crotti A., Benner C., Kerman BE, Gosselin D., Lagier-Tourenne C., Zuccato C., Cattaneo E., Gage FH, Cleveland DW, and Glass CK (2014). Generation of a transgenic mouse model with chondrocyte-specific and tamoxifen-inducible expression of Cre recombinase. Genesis 17, 513–521. 10.1002/dvg.20261.Generation.
57. Ryan HE, Poloni M., McNulty W., Elson D., Gassmann M., Arbeit JM, and Johnson RS (2000). Hypoxia-inducible factor-1alpha is a positive factor in solid tumor growth. Cancer Res. 60, 4010–4015. [PubMed: 10945599]
58. Shultz LD, Lyons BL, Burzenski LM, Gott B., Chen X., Chaleff S., Kotb M., Gillies SD, King M., Mangada J., et al. (2005). Human lymphoid and myeloid cell development in NOD/LtSz-scid IL2R γ null mice engrafted with mobilized human hemopoietic stem cells. J. Immunol. 174, 6477–6489. 10.4049/jimmunol.174.10.6477. [PubMed: 15879151]
59. Wu C., Wei Q., Utomo V., Nadesan P., Whetstone H., Kandel R., Wunder JS, and Alman BA (2007). Side population cells isolated from mesenchymal neoplasms have tumor initiating potential. Cancer Res. 67, 8216–8222. 10.1158/0008-5472.CAN-07-0999. [PubMed: 17804735]
60. Rasheed S., Nelson-Rees WA, Toth EM, Arnstein P., and Gardner MB (1974). Characterization of a newly derived human sarcoma cell line (HT-1080). Cancer 33, 1027–1033. 10.1002/1097-0142. [PubMed: 4132053]
61. Jagasia AA, Block JA, Qureshi A., Diaz MO, Nobori T., Gitelis S., and Iyer AP (1996). Chromosome 9 related aberrations and deletions of the CDKN2 and MTS2 putative tumor suppressor genes in human chondrosarcomas. Cancer Lett. 105, 91–103. 10.1016/0304-3835(96)04274-7. [PubMed: 8689637]
62. Goldring MB, Birkhead JR, Suen LF, Yamin R, Mizuno S, Glowacki J, Arbiser JL, Apperley JF Interleukin-1,8-modulated gene expression in immortalized human chondrocytes. J. Clin. Invest. 94 2307–2316
63. Zhang H., Wei Q., Tsushima H., Puviindran V., Tang YJ, Pathmanapan S., Poon R., Ramu E., Al-Jazrawe M., Wunder J., and Alman BA (2019). Intracellular cholesterol biosynthesis in enchondroma and chondrosarcoma. JCI Insight 5, e127232. 10.1172/jci.insight.127232.

Author Manuscript Author Manuscript Author Manuscript Author Manuscript

Highlights

- Mutant *IDH* chondrosarcomas and mutant *Idh1* mice harbor elevated levels of glycogen
- Glycogen fuels tumor growth and downstream energetic pathways
- *Gys1* deletion reduces enchondroma-like lesion formation in mutant *Idh1* mice
- HIF1α and mutant IDH1 interact to regulate glycogen metabolism in tumor cells

Author Manuscript Author Manuscript Author Manuscript Author Manuscript

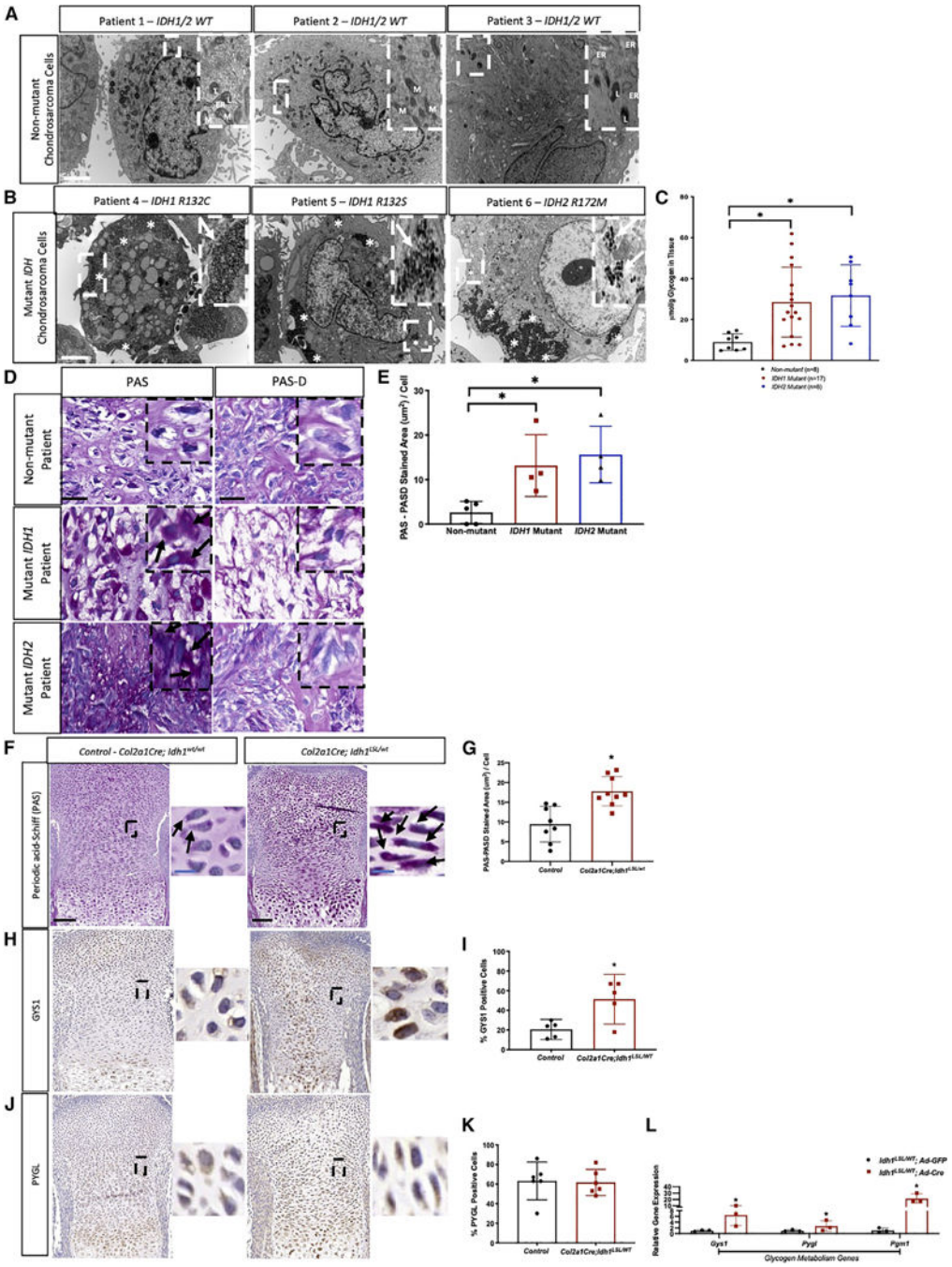

Figure 1. Glycogen levels are elevated in mutant *IDH* chondrosarcoma patient tissue and in the mutant *Idh1-KI R132Q* fetal growth plate

(A) Transmission electron microscopy (TEM) images of *IDH* non-mutant chondrosarcoma cells (n = 4) *in vitro* display absent glycogen granules. Organelles distinct from glycogen granules shown in magnified insets labeled as follows: M, mitochondria; L, lysosome; ER, rough endoplasmic reticulum. TEM images: 7× magnification, inset images: 70× magnification.

(B) TEM images of mutant *IDH* chondrosarcoma cells (n = 7) display glycogen pools, asterisks denote aggregates of glycogen pools in mutant *IDH* cells, and arrows in magnified

Author Manuscript Author Manuscript Author Manuscript Author Manuscript

insets indicate glycogen pools. Glycogen appears as closely packed circular granules in mutant *IDH* chondrosarcoma patient cells. Images: 7× magnification, inset images: 70× magnification.

(C) Glycogen quantification from pulverized patient-derived xenograft chondrosarcoma tissues display an elevation of glycogen in mutant *IDH1* (n = 17) and *IDH2* (n = 8) tumors compared with non-mutant tumors (n = 8). One-way ANOVA confirms significant statistical difference of glycogen levels between tumor genotypes ($F(2,30) = 6.150$, $p = 0.0058$). Tukey's multiple comparisons test indicates that the mean values of glycogen in mutant IDH1 ($p = 0.0107$) and mutant IDH2 groups ($p = 0.0109$) were significantly higher than in non-mutant tumors.

(D) PAS staining identified glycogen deposits in mutant *IDH1* (n = 4) and *IDH2* (n = 4) patient chondrosarcomas compared with non-mutant tumors (n = 5). PAS-D staining displays dissolution of glycogen deposits in mutant *IDH* tumors, thus confirming the presence of glycogen deposits. Arrows in magnified insets indicate glycogen deposits in cytoplasm of cells. Images: 40× magnification, inset images: 60× magnification.

(E) Quantification of PAS-stained area (μm^2), normalized to total number of cells, and of PAS-D-stained area shows an elevation of glycogen deposits in mutant *IDH1* (n = 4) and *IDH2* (n = 4) chondrosarcomas compared with non-mutant tumors (n = 5). One-way ANOVA confirms significant statistical difference of glycogen levels between tumor genotypes ($F(2,10) = 7.537$, $p = 0.0101$). Tukey's multiple comparisons test indicates mean values of glycogen in mutant *IDH1* ($p = 0.0380$) and mutant IDH2 groups ($p = 0.0123$) were significantly higher than non-mutant tumors.

(F) Glycogen deposits in *Col2a1Cre; Idh1*$^{LSL/wt}$ E18.5 growth plates (n = 9) shown by PAS staining. Arrows in magnified insets indicate glycogen in cell cytoplasm. Glycogen deposits minimally in *Col2a1Cre; Idh1*$^{wt/wt}$ control growth plates (n = 8).

(G) Quantification of PAS-stained area (μm^2), normalized to total number of cells, and PAS-D-stained area (n = 8).

(H) GYS1 staining is elevated in *Col2a1Cre; Idh1*$^{LSL/wt}$ growth plates compared with *Col2a1Cre; Idh1*$^{wt/wt}$ growth plates (n = 5).

(I) Quantification of GYS1 staining from hypertrophic to resting zones (n = 5).

(J) PYGL staining is unchanged in *Col2a1Cre; Idh1*$^{LSL/wt}$ and *Col2a1Cre; Idh1*$^{wt/wt}$ growth plates (n = 6).

(K) Quantification of PYGL staining from hypertrophic to resting zones (n = 6).

(L) Gene expression levels of glycogen genes are elevated upon *Idh1* mutation induced by adenovirus Cre recombinase transfection (n = 3). Relative gene expression compared with adenovirus GFP control group was calculated and normalized to β-actin using the $2^{-\Delta\Delta Ct}$ method. One-way ANOVA with Tukey's multiple comparisons test = $p < 0.05$. p value = Student's t test $p < 0.05$, an asterisk (*) indicates that significant p values are shown. Means and error bars representing standard deviations are shown. Scale bars: 2 μm in white, 100 μm in black, and 10 μm in blue. Magnification: whole growth plate images: 13× magnification, inset images: 60× magnification.

Author Manuscript Author Manuscript Author Manuscript Author Manuscript

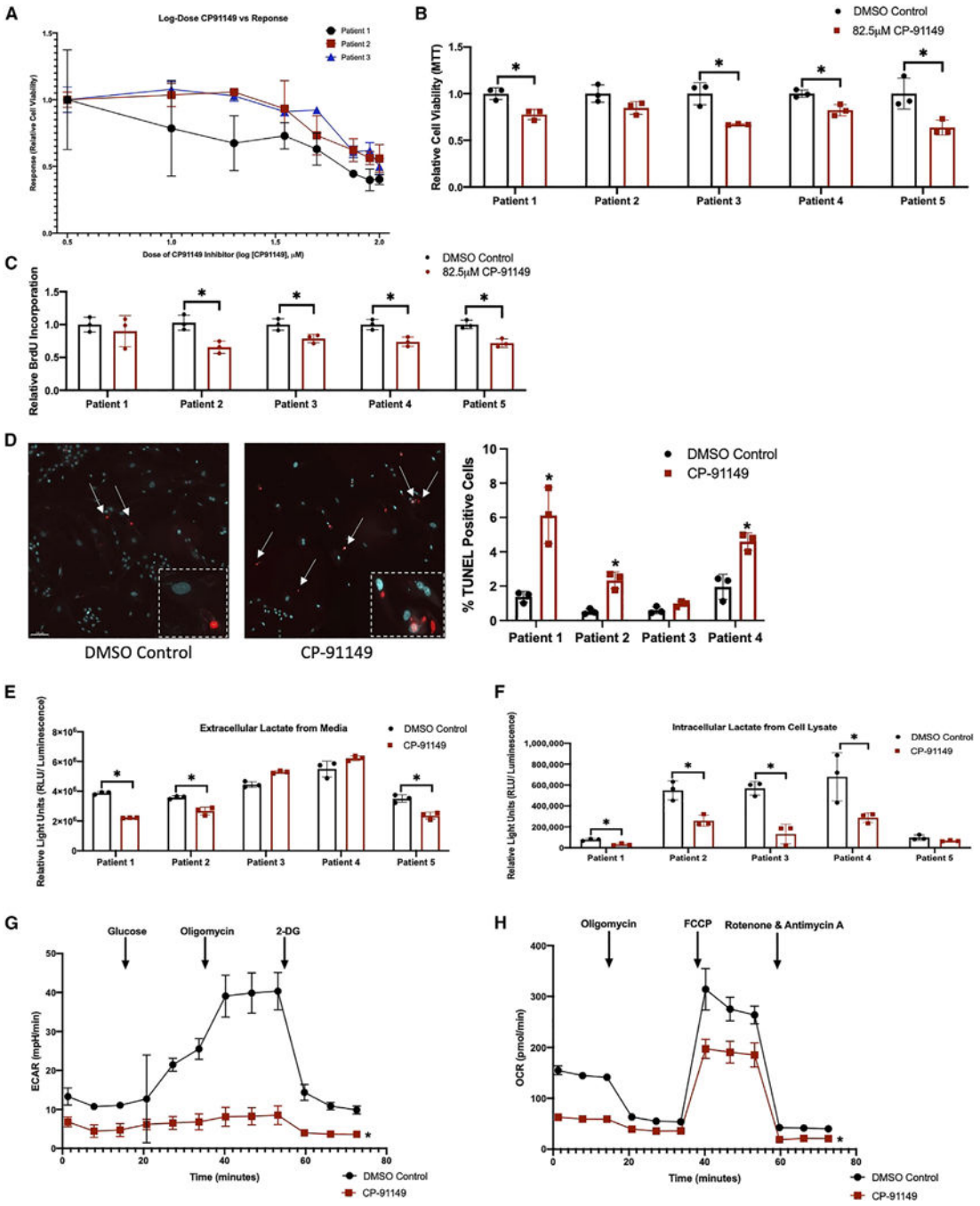

Figure 2. Glycogen utilization fuels glycolysis and oxidative phosphorylation in mutant *IDH* chondrosarcomas and promotes tumor cell viability, proliferation, and survival

(A) Glycogenolysis enzymic activity (PYGL) was inhibited with CP-91149 drug. Increasing concentrations of CP-91149 induced sensitivity to primary patient mutant *IDH* chondrosarcoma cells as displayed by the dose-response curve (n = 3).

(B) 82.5 μM CP-91149 reduced cell viability in 4 patient cell lines (n = 3).

(C) Glycogenolysis blockade reduced BrdU incorporation (cell proliferation) in 4 out of 5 cell lines (n = 3).

Author Manuscript Author Manuscript Author Manuscript Author Manuscript

(D) Glycogenolysis blockade induced apoptosis in 3 out of 4 cell lines (n = 3). Arrows indicate TUNEL-positive stained cells. 103 magnification.
(E and F) PYGL blockade reduced secreted (n = 3) (E) and intercellular (F) lactate levels, suggesting that glycogen utilization fuels glycolysis (n = 3).
(G) PYGL blockade reduced glycolytic (n = 3) (G) and oxidative (H) capacities of chondrosarcoma cells (n = 3). p value = Student's t test $p < 0.05$, an asterisk (*) indicates that significant p values are shown. Means and error bars representing standard deviations are shown. Scale bars: 100 μm in white.

Author Manuscript Author Manuscript Author Manuscript Author Manuscript

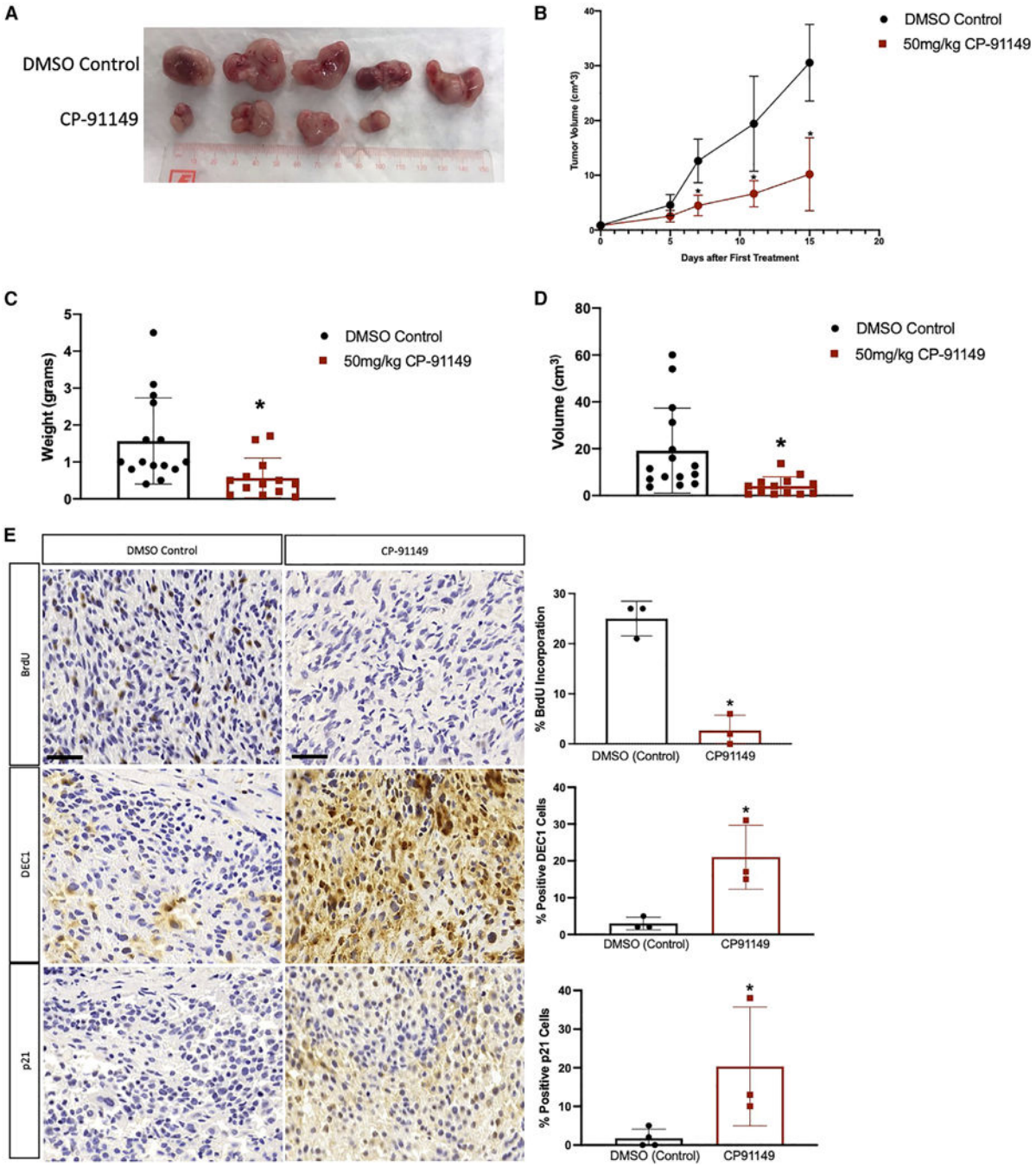

Figure 3. Pharmacological blockade of glycogen utilization (PYGL) impairs chondrosarcoma tumor growth *in vivo*, reduces proliferation, and induces cellular senescence in glycogen-deprived tumors

15-day treatment of PDX tumors with 50 mg/kg CP-91149 resulted in a reduction in (A) tumor size (n = 4), (B) tumor growth (n = 4), (C) tumor weight (n = 14), and (D) tumor volume (n = 14).

(E) BrdU staining (n = 3) of CP-91149-treated tumors revealed a reduction in BrdU incorporation, suggesting a reduction in proliferation, and an increase in DEC1 (n = 3) and p21 (n = 3) staining, suggesting glycogenolysis blockade induces cellular senescence.

p value = Student's t test $p < 0.05$, an asterisk (*) indicates that significant p values are shown. Means and error bars representing standard deviations are shown. Scale bars: 50 μm in black.

Author Manuscript Author Manuscript Author Manuscript Author Manuscript

Author Manuscript
Author Manuscript
Author Manuscript
Author Manuscript

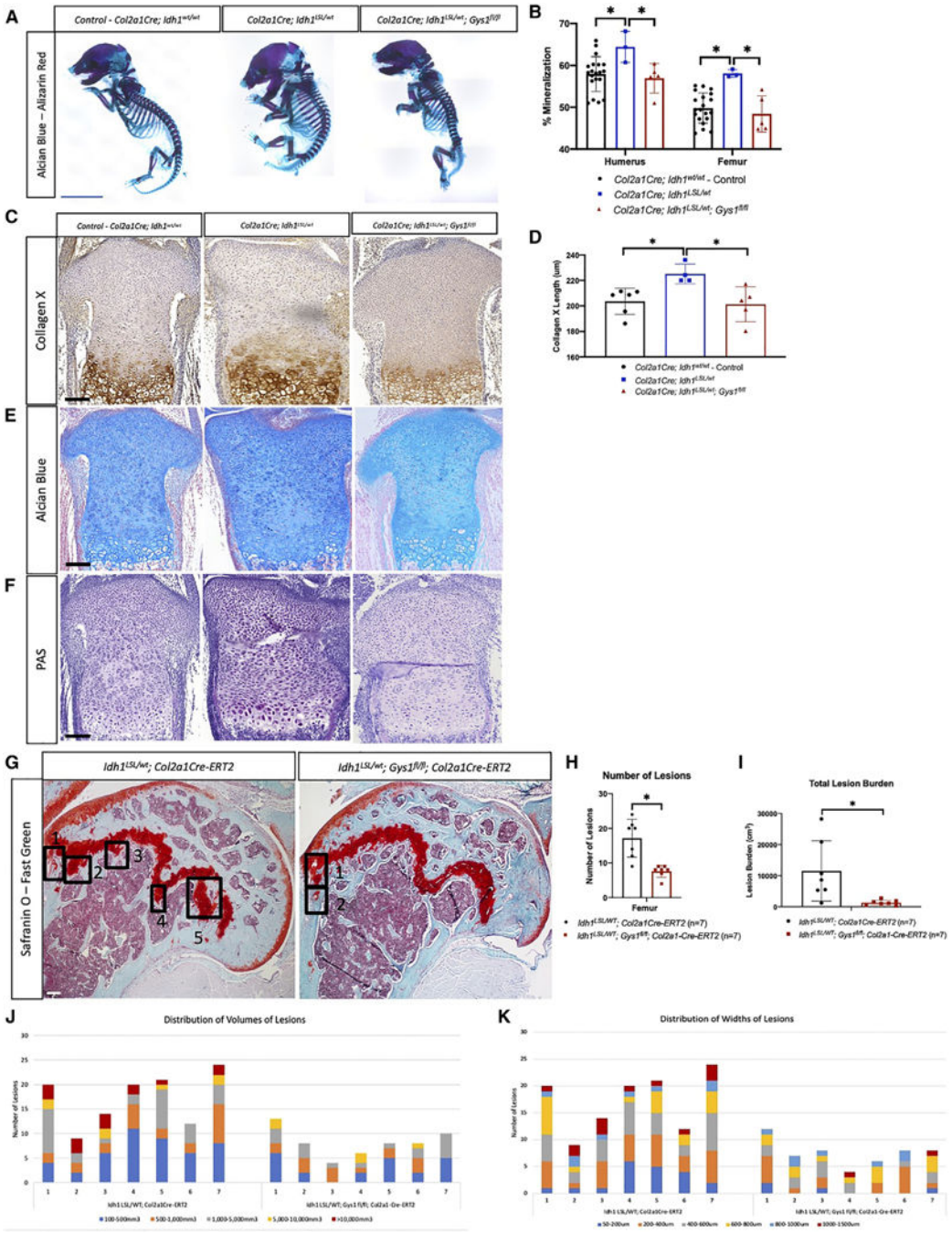

Figure 4. Cartilaginous *Idh1-KI; Gys1* deletion rescues some aspects of the *Idh1-KI* phenotype and is sufficient to reduce enchondroma-like cartilage lesions in the *Idh1-KI* growth plate

(A) Alizarin red and Alcian blue whole-mount skeleton of $Idh1^{LSL/wt}$ (n = 3), $Idh1^{LSL/wt}$; $Gys1^{fl/fl}$ (n = 5), and littermate controls (n = 20) at E18.5.

(B) Percent mineralization of humerus and femur bones of $Idh1^{LSL/wt}$ (n = 3), $Idh1^{LSL/wt}$; $Gys1^{fl/fl}$ (n = 5), and littermate control (n = 20) mice. Two-way ANOVA confirms significant statistical difference in percent mineralization in humerus and femur between genotypes ($F(6,175) = 21.76$, $p < 0.0001$). Tukey's multiple comparisons test = $p < 0.05$, an asterisk (*) indicates that significant p values are shown.

Author Manuscript Author Manuscript Author Manuscript Author Manuscript

(C) Collagen 10 (COLX) staining of *Idh1*$^{LSL/wt}$ (n = 3), *Idh1*$^{LSL/wt}$; *Gys1*$^{fl/fl}$ (n = 5), and littermate control (n = 6) growth plates.
(D) COLX stained length measurements of *Idh1*$^{LSL/wt}$, *Idh1*$^{LSL/wt}$; *Gys1*$^{fl/fl}$, and littermate control growth plates. One-way ANOVA confirms significant statistical difference in COLX height between three genotypes ($F(2,12) = 6.175$, $p < 0.0143$). Tukey's multiple comparisons test = $p < 0.05$, an asterisk (*) indicates that significant p values are shown.
(E) Alcian blue staining of *Idh1*$^{LSL/wt}$ (n = 3), *Idh1*$^{LSL/wt}$; *Gys1*$^{fl/fl}$ (n = 5), and littermate control (n = 5) tibia growth plates at E18.5.
(F) PAS staining of *Idh1*$^{LSL/wt}$ (n = 3), *Idh1*$^{LSL/wt}$; *Gys1*$^{fl/fl}$ (n = 5), and littermate control (n = 5) growth plates.
(G) Representative Safranin O staining of 5-month-old postnatal femur murine growth plates of specified genotypes. Enchondroma-like lesions are highlighted in black boxes. Representative *Col2a1Cre-ERT2; Idh1*$^{LSL/wt}$ (n = 7) femur growth plate displays 5 lesions, whereas representative *Col2a1Cre-ERT2; Idh1*$^{LSL/wt}$; *Gys1*$^{fl/fl}$ (n = 7) growth plate displays 2 lesions.
(H) Quantification of lesions in femur growth plates show that *Col2a1Cre-ERT2; Idh1*$^{LSL/wt}$; *Gys1*$^{fl/fl}$ (n = 7) animals display less lesions compared with *Col2a1Cre-ERT2; Idh1*$^{LSL/wt}$ (n = 7) animals. Each data point represents 1 animal.
(I) Total lesion burden is reduced in *Col2a1Cre-ERT2; Idh1*$^{LSL/wt}$; *Gys1*$^{fl/fl}$ animals. Each data point represents 1 animal (n = 7).
(J and K) Distribution of (J) volumes of enchondroma-like lesions and (K) widths of lesions. p value = Student's t test $p < 0.05$, an asterisk (*) indicates that significant p values are shown. Means and error bars representing standard deviations are shown. Scale bars: 5,000 μm in blue, 100 μm in black, and 100 μm in white.

Author Manuscript Author Manuscript Author Manuscript Author Manuscript

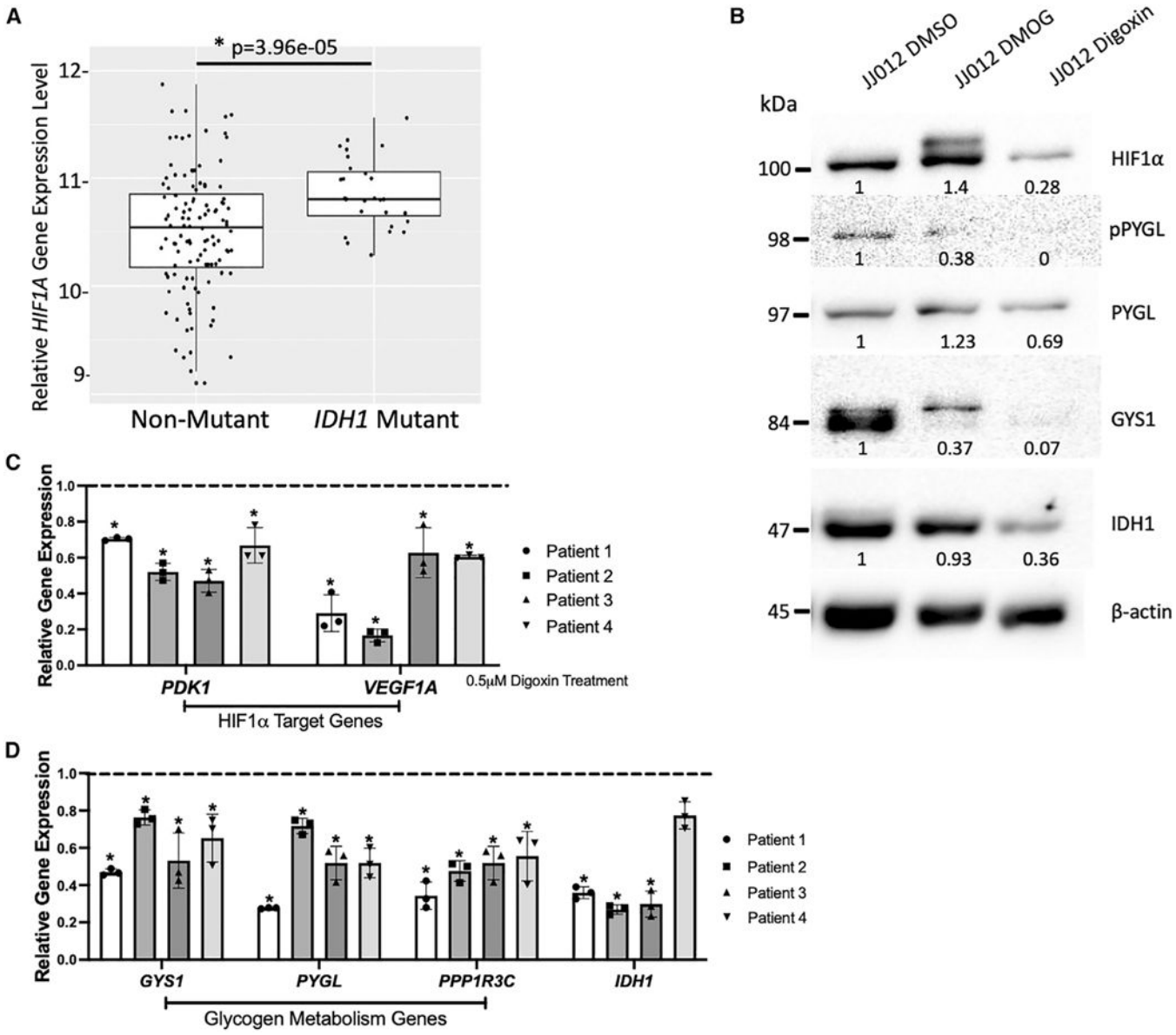

Figure 5. HIF1α transcriptionally regulates glycogen metabolism in mutant *IDH* chondrosarcomas

(A) Analysis of published gene expression data shows that HIF1α gene expression levels are elevated in mutant *IDH1* chondrosarcomas (n = 116) compared with non-mutant tumors (n = 28).

(B) Mutant *IDH1* JJ012 cells treated with 0.5 mM DMOG and 0.25 μM digoxin stabilized and depleted HIF1α, respectively. DMOG treatment displayed elevated protein levels of HIF1α and total PYGL, and digoxin treatment displayed depleted protein levels of HIF1α, total PYGL, pPYGL, GYS1, and IDH1. Quantitative densitometry analysis of relative protein expression levels are displayed beneath respective protein bands. Protein density measurements are displayed as relative measurements by normalization to β-actin protein density measurements compared with fold change to DMSO control treatment.

Author Manuscript Author Manuscript Author Manuscript Author Manuscript

(C) Primary patient chondrosarcoma cells treated with 0.5 μM digoxin display a reduction in *PDK1* and *VEGF* levels, confirming that HIF1α is depleted in cells (n = 4). Relative gene expression for four patient-derived cell cultures compared to DMSO-treated control cultures (normalized to β-actin).

(D) HIF1α depletion is sufficient to knock down gene expression levels of glycogen metabolism genes, *GYS1*, *PYGL, PPP1R3C*, and *IDH1*, suggesting that HIF1α is a regulator of glycogen metabolism (n = 4). Relative gene expression for four patient-derived cell cultures compared to DMSO-treated control cultures (normalized to β-actin). p value = Student's t test $p < 0.05$, an asterisk (*) indicates that significant p values are shown. Means and error bars representing standard deviations are shown.

Author Manuscript Author Manuscript Author Manuscript Author Manuscript

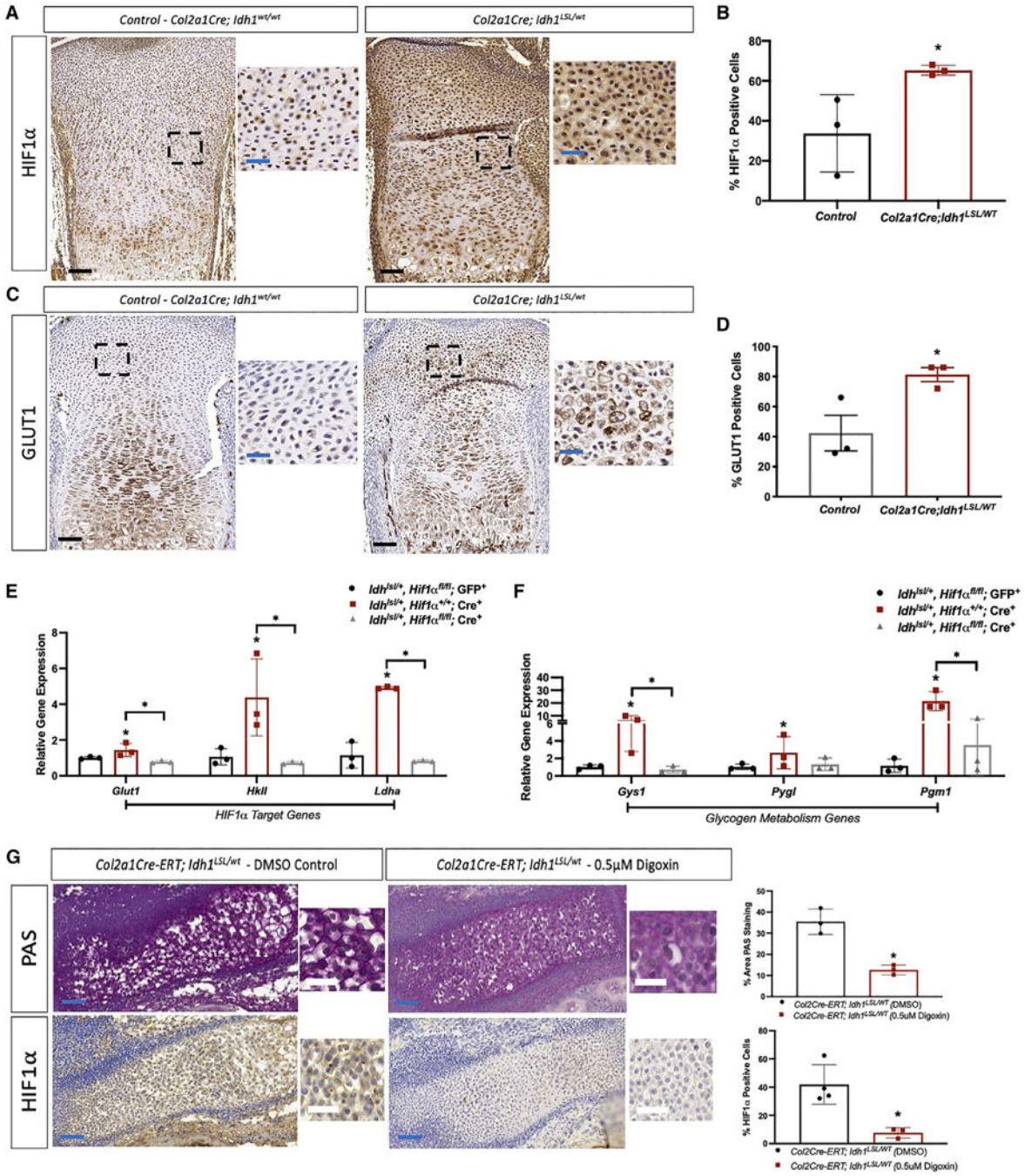

Figure 6. HIF1α regulates glycogen metabolism in *Idh1-KI* chondrocytes and in the fetal growth plate

(A) HIF1α staining is elevated in *Col2a1Cre; Idh1*$^{LSL/wt}$ E18.5 growth plates compared with *Col2a1Cre; Idh1*$^{wt/wt}$ growth plates (n = 3). Inset images taken at 20× magnification at the proliferative zone of the growth plate.

(B) Quantification of HIF1α staining from hypertrophic to resting zones (n = 3).

(C) GLUT1 staining is elevated in *Col2a1Cre; Idh1*$^{LSL/wt}$ growth plates compared with *Col2a1Cre; Idh1*$^{wt/wt}$ growth plates (n = 3). Inset images taken at 20× magnification at the proliferative zone of the growth plate.

Author Manuscript Author Manuscript Author Manuscript Author Manuscript

(D) Quantification of GLUT1 staining from hypertrophic to resting zones (n = 3).
(E) Gene expression levels of HIF1α target genes are significantly reduced upon *Idh1* mutation and HIF1α knockdown induced by adenovirus Cre recombinase transfection (n = 3).
(F) Gene expression levels of glycogen metabolism genes are significantly reduced upon *Idh1* mutation and HIF1α knockdown (n = 3).
(G) *Ex vivo* explant cultures of E16.5 *Col2a1Cre-ERT; Idh1*$^{LSL/wt}$ metatarsals display reduced glycogen (PAS) and HIF1α levels upon pharmacological blockade of HIF1α by 0.5 μM digoxin treatment for 4 days (n = 6). Inset images are taken at 15× magnification at the central area of the growth plate. p value = Student's t test $p < 0.05$, an asterisk (*) indicates that significant p values are shown. Means and error bars representing standard deviations are shown. Scale bars: 100 μm in black, 50 μm in blue, and 20 μm in white.

Author Manuscript Author Manuscript Author Manuscript Author Manuscript

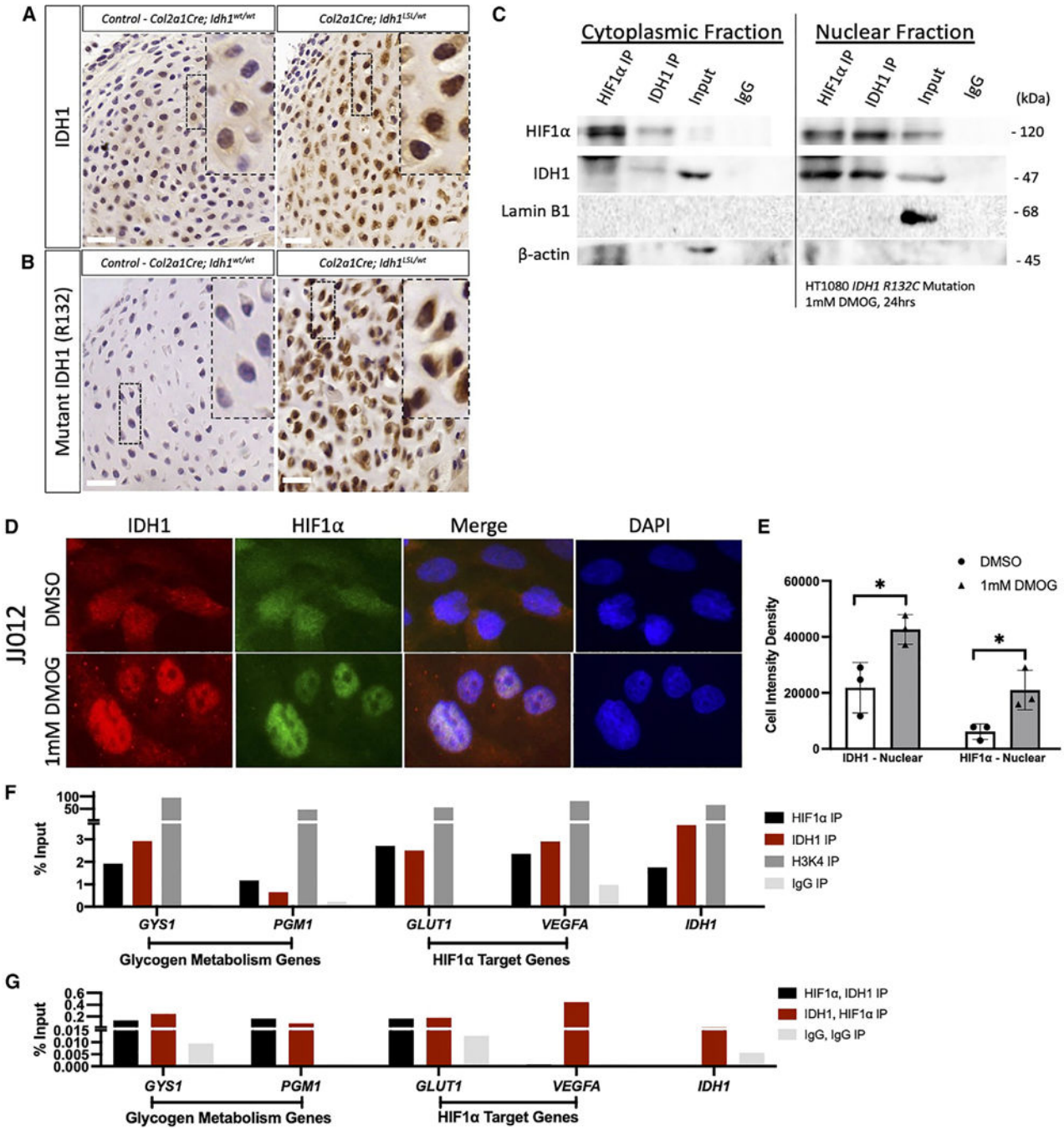

Figure 7. *HIF1α* and mutant *IDH1* interact to regulate glycogen metabolism in mutant *IDH* chondrosarcomas

(A) Immunohistochemistry (IHC) staining of mutant IDH1 in mutant *Idh1*^{R132Q} growth plates (n = 3) displays weak cytoplasmic and strong nuclear staining, whereas control growth plates (n = 3) display weak cytoplasmic staining of IDH1.

(B) IHC staining of mutant IDH1 R132— in mutant *Idh1*^{R132Q} growth plates (n = 3) displays strong cytoplasmic and strong nuclear staining, whereas control growth plates (n = 3) display no staining of mutant IDH1.

Author Manuscript Author Manuscript Author Manuscript Author Manuscript

(C) Mutant *IDH1*^{R132C} tumor cell line, HT1080, shows that HIF1α interacts with mutant IDH1 in the nuclear fraction as shown in HIF1α IP and IDH1 IP lanes. HIF1α and mutant IDH1 interact minimally in the cytoplasmic fraction.
(D) JJ012 mutant *IDH1*^{R132G} cells display nuclear localization of mutant IDH1 and co-localization with HIF1α in hypoxic conditions (n = 7). 40× magnification.
(E) Quantitative cell intensity measurements of JJ012 mutant *IDH1*^{R132G} cell line confirms significant nuclear localization of mutant IDH1 and co-localization of HIF1α in DMOG-treated cells.
(F) Individual ChIP of HIF1α and mutant IDH1 in mutant *IDH1*^{R132G} JJ012 chromatin displays enrichment of HIF1α and mutant IDH1 of glycogen metabolism and HIF1α target gene promoters containing the HRE.
(G) ChIP-re-ChIP of HIF1α, mutant IDH1 and mutant IDH1, HIF1α in mutant *IDH1*^{R132G} JJ012 chromatin displays enrichment of glycogen metabolism and HIF1α target genes. Scale bars: 20 μm in white. p value = Student's t test $p < 0.05$, an asterisk (*) indicates that significant p values are shown. Means and error bars representing standard deviations are shown. Detail on methods: the IDH1 antibody (see Table S2) used for immunostaining is specific to the immunogen around the Arg222 amino acid site of the IDH1 protein, which is distant from the Arg132 mutation site. Thus, this IDH1 antibody recognizes both wild-type IDH1 and mutant IDH1 proteins.

Author Manuscript Author Manuscript Author Manuscript Author Manuscript

KEY RESOURCES TABLE

REAGENT or RESOURCE	SOURCE	IDENTIFIER
Antibodies		
Rabbit monoclonal anti-GYS1	Cell Signaling Technology	3886S, RRID:AB_2116392
Rabbit polyclonal anti-PYGL	Abcam	ab223788
Rabbit polyclonal anti-GLUT1	Abcam	ab15309, RRID:AB_301844
Rabbit polyclonal anti-HIF1A	Novus Biologicals	NB100–479, RRID:AB_10000633
Mouse monoclonal anti-Collagen X	Thermo Fisher Scientific	14–9771-82, RRID:AB_2573018
Mouse monoclonal anti-BrdU	Novus Biologicals	NB500–439, RRID:AB_10000514
Mouse monoclonal anti-p21	Novus Biologicals	NBP2–29463
Rabbit polyclonal anti-DEC1	Novus Biologicals	NB100–1800, RRID:AB_10000524
Mouse monoclonal anti-mutant IDH1 R132-	Sigma-Aldrich	MABC1103
Mouse monoclonal anti-IDH1	Novus Biologicals	NBP1–47804, RRID:AB_10010774
Mouse monoclonal anti-P53	Thermo Fisher Scientific	AHO0152, RRID:AB_1501890
Rabbit monoclonal anti-pPYGL	Abcam	ab227043
Mouse monoclonal anti-beta actin	Sigma-Aldrich	A2228, RRID:AB_476697
Rabbit polyclonal anti-Lamin B1	Abcam	ab16048, RRID:AB_443298
Mouse monoclonal anti-HIF1A	Abcam	ab1, RRID:AB_296474
Rabbit monoclonal anti-IDH1	Cell Signaling Technology	Cat# 8137, RRID:AB_10950504
Rabbit polyclonal anti-IDH1	Thermo Fisher Scientific	PA5–28206, RRID:AB_2545682
Rabbit polyclonal anti-H3K4	Abcam	ab8580, RRID:AB_306649
Normal Rabbit IgG	Cell Signaling Technology	2729, RRID:AB_1031062
Goat anti-rabbit IgG, biotinylated	Vector Laboratories	BA-1000–1.5
Goat anti-mouse IgG, biotinylated	Vector Laboratories	BA-9200–1.5
Goat anti-mouse IgG (HRP)	Abcam	ab205719, RRID:AB_2755049
Goat anti-rabbit IgG (HRP)	Abcam	ab205718, RRID:AB_2819160
Goat anti-rabbit IgG Alexa Fluor 488	Abcam	ab150077, RRID:AB_2630356
Goat anti-mouse IgG Alexa Fluor 488	Abcam	ab150113, RRID:AB_2576208
Goat anti-rabbit IgG Alexa Fluor 674	Abcam	ab150079, RRID:AB_2722623
Goat anti-mouse IgG Alexa Fluor 674	Abcam	ab150115, RRID:AB_2687948

Cell Rep. Author manuscript; available in PMC 2023 October 23.

Author Manuscript Author Manuscript Author Manuscript Author Manuscript

REAGENT or RESOURCE	SOURCE	IDENTIFIER
Biological samples		
Primary patient human chondrosarcoma tissues	Mount Sinai Hospital, Sarcoma Tumor Bank	N/A
Mouse liver tissue	NOD scid gamma (NSG) mice from UHN Animal Resource Center	N/A
Human muscle tissue	Mount Sinai Hospital, Sarcoma Tumor Bank	N/A
Chemicals, peptides, and recombinant proteins		
Tamoxifen, 4-Hydroxy-, (Z)-	Sigma-Aldrich	579002
Progesterone	Thermo Fisher Scientific	AC225650050
Dulbecco's Modified Eagle Medium(DMEM)	Wisent Bioproducts	319–005-EL
Fetal bovine serum (FBS)	Wisent Bioproducts	080–150
Antibiotic-Antimycotic (ABAM)	Thermo Fisher Scientific	15240062
Dimethyloxallyl Glycine (DMOG)	Cayman Chemical	71210
Digoxin	Cayman Chemical	22266
Dimethyl sulfoxide (DMSO)	Thermo Fisher Scientific	85190
cOmplete protease inhibitor	Roche	11873580001
Restore PLUS Western Blot Stripping Buffer	Thermo Fisher Scientific	46430
CP-91149	Selleckchem	S2717
BrdU labeling reagent	Thermo Fisher Scientific	000103
DAPI Solution	Thermo Fisher Scientific	62248
Mutant IDH1 inhibitor	Selleckchem	S8206
Matrigel	Corning	356234
Permount	Thermo Fisher Scientific	SP15–500
Pronase	Roche	11459643001
Collagenase D	Thermo Fisher Scientific	11088882001
Collagenase IV	Worthington Biochemical Corporation	LS004189
Dispase	Thermo Fisher Scientific	17105041
Trypsin	Wisent Bioproducts	325240EL
ImmunoBlot PVDF membrane	Bio-Rad	1620177
Nitrocellulose membranes	Thermo Fisher Scientific	88024
Alpha minimum essential medium (*a*MEM)	Thermo Fisher Scientific	12571063
Penicillin streptomycin (P/S)	Thermo Fisher Scientific	15140122

Author Manuscript Author Manuscript Author Manuscript Author Manuscript

REAGENT or RESOURCE	SOURCE	IDENTIFIER
Ascorbic acid	Thermo Fisher Scientific	AC105021000
B-glycerophosphate	Cayman Chemical	14405
Bovine serum albumin (BSA)	Thermo Fisher Scientific	11020021
Nuclear fast red counterstain	Vector Laboratories	H3403500
Weigert's Iron Hematoxylin	Abcam	ab245882
Dynabeads Protein G	Thermo Fisher Scientific	10003D
Pierce Protein A Magnetic Beads	Thermo Fisher Scientific	88845
Normal Goat Serum	Thermo Fisher Scientific	31872
Avidin/Biotin Blocking Kit	Vector Laboratories	SP2001
16% Paraformaldehyde	Thermo Fisher Scientific	043368.9L
Fluoroshield mounting medium	Abcam	ab104135
Formaldehyde	Millipore Sigma	1040021000
Proteinase K	Thermo Fisher Scientific	AM2542
ABC reagent	Vector Laboratories	PK-4000
DAB solution	Vector Laboratories	SK-4100
Critical commercial assays		
DNeasy Blood and Tissue Kit	Qiagen	69504
KOD Hot Start DNA Polymerase	Sigma-Aldrich	71086–3
QIAquick PCR Purification Kit	Qiagen	28104
Abcam Glycogen Assay Kit II	Abcam	ab169558
Pierce BCA Protein Assay Kit	Thermo Fisher Scientific	23227
Immobilon Forte Western HRP substrate	Millipore	WBLUF0100
Norgen Biotek Corp Single Cell RNA Isolation Kit	Norgen Biotek Corp	51800
BioRad iScript	BioRad	1708890
SsoAdvanced Universal SYBR Green Supermix	BioRad	1725272
Trevigen TACs MTT Cell Proliferation Assay	R&D Systems	4890–025-K
Cell Proliferation ELISA, BrdU Kit	Roche	11647229001
In Situ Cell Death Detection Kit, TMR red	Roche	12156792910
Lactate-Glo Assay	Promega	J5021
NE-PER Nuclear and Cytoplasmic Extraction Kit	Thermo Fisher	78833

Author Manuscript Author Manuscript Author Manuscript Author Manuscript

REAGENT or RESOURCE	SOURCE	IDENTIFIER
Deposited data		
mRNA profiling by array of cartilage tumors[27] (analysis of existing, publicly available data)	E-MTAB-7264[28] PMID: 31604924 [52] PMID: 20688976	https://www.ebi.ac.uk/biostudies/arrayexpress/studies/E-MTAB-7264
Experimental models: Cell lines		
Primary chondrosarcoma cell lines	This paper	N/A
HT1080	ATCC	CCL-121
JJ012	Dr. Joel A Block, Rush University	RRID: CVCL_D605
C28/I2 Human Chondrocytes	Sigma-Aldrich	SCC043
Experimental models: Organisms/strains		
Mouse: *Gys1$^{fl/fl}$*	Duran et al.[53]	N/A
Mouse: *Idh1-KI R132Q*	Sasaki et al.[54] Hirata et al.[10]	N/A
Mouse: *Col2a1Cre*	Long et al.[55]	N/A
Mouse: *Col2a1Cre-ERT2*	Crotti et al.[56]	N/A
Mouse: *Col2a1Cre-ERT*	The Jackson Laboratory, Bar Harbor, ME	006774, RRID:IMSR_JAX:006774
Mouse: *Hif1α$^{fl/fl}$*	Ryan et al.[57]	N/A
Mouse: NOD scid gamma (NSG)	UHN Animal Resource Center	N/A
Oligonucleotides		
Primers PCR amplification of human exon 4 IDH1/IDH2 see Table S1	Sasaki et al.[54] Hirata et al.[10]	N/A
Primers human IDH1/IDH2 R132-mutation sequencing see Table S1	Sasaki et al.[54] Hirata et al.[10]	N/A
Primers of genes mRNA transcripts, human, RT-qPCR see Table S3	This paper	N/A
Primers of genes mRNA transcripts, mouse, RT-qPCR see Table S3	This paper	N/A
Primers ChIP re-ChIP RT-qPCR, human, representing potential HIF1a, mutant IDH1 binding sites in gene promoter regions see Table S4	This paper	N/A

Author Manuscript Author Manuscript Author Manuscript Author Manuscript

REAGENT or RESOURCE	SOURCE	IDENTIFIER
Recombinant DNA		
Ad-CMV-Cre Cre recombinase adenovirus co-expression with GFP	Vector Biolabs	1700
Ad-GFP Control	Vector Biolabs	1060
Software and algorithms		
4Peaks software	Softonic	https://4peaks.en.softonic.com/mac?ex=DINS-635.2
R v3.4.4	“survminer” package	https://cran.r-project.org/
Prism GraphPad 9	GraphPad Software	https://www.graphpad.com/
CaseViewer	3DHistech Ltd.	https://www.3dhistech.com/solutions/caseviewer/
ImageJ	ImageJ Software	https://imagej.nih.gov/ij/download.html
Other		
FEI Tecnai 20 transmission electron microscope	FEI Tecnai	N/A
Nikon Eclipse E1000 microscope	Nikon	N/A
NCBI PrimerBLAST	NCBI	https://www.ncbi.nlm.nih.gov/tools/primer-blast/
Ensembl genome browser 109	EMBL-EBI	https://useast.ensembl.org/index.html
Agilent Seahorse XF96 analyzer	Agilent	N/A
Diagenode Bioruptor Sonicator	Diagenode	N/A

Cell Rep. Author manuscript; available in PMC 2023 October 23.